

Root zone soil moisture mapping at very high spatial resolution using radar-derived surface soil moisture product

Nadia Ouaadi^{a,*}, Abdelghani Chehbouni^a, Emna Ayari^b, Bouchra Ait Hssaine^a,
Jamal ElFarkh^a, Michel Le Page^d, Salah Er-Raki^{a,c}, Aaron Boone^e

^a CRSA, Mohammed VI Polytechnic University, Ben Guerir, Morocco

^b VPE, Swedish University of Agricultural Sciences, Umeå, Sweden

^c CAB, Centre AgroBiotech-URL-CNRST-05, Cadi Ayyad University, Marrakech, Morocco

^d CESBIO, University of Toulouse, IRD/CNRS/UPS/CNES, Toulouse, France

^e GMME/SURFACE, Météo-France/CNRM, Toulouse, France

ARTICLE INFO

Handling Editor: Dr Z Xiyang

Keywords:

Root zone soil moisture
Surface soil moisture
Radar remote sensing
Exponential filter
Crops

ABSTRACT

Root zone soil moisture (RZSM) is a key variable controlling the soil-vegetation-atmosphere exchanges. Its estimation is vital for monitoring hydrological, meteorological and agricultural processes. A number of large-scale products exist but with a coarse resolution (>1 km), which is not suitable for plot-scale studies. The aim of this work is to map RZSM, for the first time, at very high spatial resolution using a very high spatial resolution surface soil moisture (SSM) product and a recursive exponential filter. SSM is estimated from Sentinel-1 data using the water cloud model at a resolution of approximately 50 m. The approach was evaluated on a database consisting of 12 fields, including 7 winter wheat and 5 summer maize fields, irrigated using different techniques. The results show that the approach performs reasonably well using Sentinel-1 SSM product with correlation coefficient (R) between 0.3 and 0.82, root-mean-square error (RMSE) between 0.05 and 0.12 m³/m³ and a bias in the range -0.1–0.07 m³/m³, at 15–20 cm depth. This is equivalent to R = 0.6, RMSE = 0.12 m³/m³ and bias = 0.07 m³/m³ using the entire database, which is quite low compared to the use of in situ SSM measurements (R = 0.81, RMSE = 0.07 m³/m³ and bias = 0.03 m³/m³). This is related to inaccuracies in the SSM product, where fields with good SSM estimation also resulted in good RZSM estimation and conversely. In addition to SSM, the approach is also sensitive to its time constant T. Analysis of RZSM sensitivity to T shows that the optimum T value depends on soil texture, climate and measurement depth. In particular, low optimum T values (1 day) are obtained for loamy and sandy loam soils, while higher values (5–10 days) are optimal for soils with a high clay fraction, at 15–20 cm depth. These values increase with soil depth and are influenced by seasonal atmospheric demand. Combined to reasonable statistical metrics, the spatial variability depicted by the RZSM maps opens up prospects for high-resolution RZSM mapping from Sentinel-1 SSM data using a simple approach over annual crops. This is of prime relevance for agricultural applications requiring very high-resolution estimation at plot scale, such as crop yield, irrigation and fertilizer management, as well as for the assessment of inter-plot variability.

1. Introduction

Water resources are a limiting factor for development in the majority of countries worldwide (Ferguson et al., 2018). An optimal management is considered as a source of peace and prosperity (United Nations, 2024). This management concerns particularly agriculture, where irrigation consumes up to 90 % of available resources in several Mediterranean regions, which additionally experience a pronounced amplification of

extreme events (IPCC, 2019; MedECC, 2020). Optimal irrigation is therefore essential to improve water use efficiency, reduce costs and minimize environmental impact (McDermid et al., 2023).

Root zone soil moisture (RZSM) directly influences land-atmosphere interactions (Ford et al., 2014; Koster et al., 2004; Taylor et al., 2007), water requirements (Alfieri et al., 2008; Ford et al., 2014; Kim et al., 2023), and therefore irrigation scheduling (Blonquist et al., 2006; Fontanet et al., 2018; Massari et al., 2021). It is also an important variable

* Corresponding author.

E-mail address: nadia.ouaadi@um6p.ma (N. Ouaadi).

<https://doi.org/10.1016/j.agwat.2025.109507>

Received 20 January 2025; Received in revised form 21 April 2025; Accepted 23 April 2025

Available online 29 April 2025

0378-3774/© 2025 The Authors. Published by Elsevier B.V. This is an open access article under the CC BY license (<http://creativecommons.org/licenses/by/4.0/>).

for many other hydrological, agronomic and meteorological studies (Brakhasi et al., 2023; Chen et al., 2018; Das et al., 2006; Jiang et al., 2021; Sabater et al., 2007; Valayamkunnath et al., 2019; Vereecken et al., 2008). Typically, RZSM can be estimated using in situ sensors, mainly Time Domain Reflectometry (TDR) and thetaprobes (Dobriyal et al., 2012; Noborio, 2001; Vereecken et al., 2008; Zreda et al., 2012). Although accurate, the sensors can only give point information, whereas the spatio-temporal variability of RZSM requires a network of sensors. However, the installation and monitoring/maintenance of a large network is tedious, time-consuming, costly and is likely to disturb soil properties (Brakhasi et al., 2023; Carranza et al., 2021).

Remote sensing data can provide global and frequent mapping of observable variables such as surface soil moisture (SSM). Indeed, there are a large number of SSM products available worldwide (e.g., Entekhabi et al., 2010; Kerr et al., 2001; Njoku et al., 2003; Wagner et al., 2003). Note that all these products are derived from microwaves because of the signal's sensitivity in this domain to the target's water content. Indeed, the microwave scattering mechanism of a medium composed of soil and vegetation is determined by its dielectric properties. Below 10 GHz, the dielectric constant of a plant cover is dominated by that of water: around 80, whereas it is around 3 for dry plant matter and dry soil (Carlson, 1967; Dobson and Ulaby, 1986; Ulaby, 1984).

Estimating RZSM is, however, more challenging than SSM, first because it is not an observable variable, i.e. directly related to satellite observations. Second, even with some sensors that can reach the root zone (long wavelengths such as P-band), scattering models for depth are more complex as the processes of wave interaction with the subsurface medium are also involved, resulting in a complex mathematical modeling scheme with a high number of input variables for both direct and inverse problems (Etminan et al., 2020). Consequently, the estimation of RZSM always incorporates a modeling approach that establishes a link between surface-related remote sensing observations, typically SSM, and RZSM. Indeed, SSM is commonly used to estimate RZSM, thanks to the strong relationship between soil moisture at the surface and in the root zone identified since the early 80 s (Camillo and Schmugge, 1983; Ford et al., 2014; Mahmood et al., 2012). The RZSM estimation approaches can be classified into four main categories: physical, semi-empirical, empirical and machine learning models (Kostov and Jackson, 1993; Li et al., 2023). The physical approaches are based on the combination of remotely sensed SSM with physical model simulations (hydrological or land surface model) using a data assimilation approach (sequential or variational methods) for providing a more accurate RZSM estimate than that obtained by the model simulation alone (Das and Mohanty, 2006; Dumedah et al., 2015; Khandan et al., 2022; Vereecken et al., 2008). It is regarded as the most promising and accurate method for estimating RZSM (e.g., Li et al. 2023). However, this approach is also associated with complex and uncertain data assimilation methods and physical models, in addition to the large amount of required input data (Liu et al., 2024; Van Oorschot et al., 2021). Empirical approaches instead rely on establishing simple relationships between RZSM and SSM. They are simple but lack representativeness and therefore cannot be applied on a large scale as the relationships are site-specific and therefore affected by climate, vegetation type, soil texture and properties. Rather better, machine learning algorithms can be used to extract RZSM by data learning and training remote sensing datasets including SSM with other variables related to vegetation type and soil properties (Carranza et al., 2021). They have been widely used (Babaeian et al., 2021; Namdari et al., 2024; Souissi et al., 2022) but still face the challenge of balancing accuracy of estimation, selection of training features, computation time and ease of interpretation and relating results to model features (Carranza et al., 2021; Montavon et al., 2018; Prasad et al., 2018; Reichstein et al., 2019). In addition, the environmental conditions and characteristics of the data used for training have a major impact on the accuracy of the approach when extrapolating to other regions with different conditions (Ayari et al., 2024; Li et al., 2023; Zeng et al., 2019). Finally, semi-empirical

models are based on physical mechanisms in which certain processes are simplified using data and empirical relationships, making them better able to balance complexity and estimation accuracy. The most popular semi-empirical model for estimating RZSM is the exponential filter, which is based on describing the infiltration process of SSM towards the root zone with an exponential form (Wagner et al., 1999). The approach requires SSM, a time constant parameter that can be calibrated, a minimum and maximum soil wetness values that can be derived from field capacity, wilting point and total water capacity. Note that a number of studies have defined the two soil wetness values, allowing transition from the soil water index to SSM, at the minimum and maximum of the SSM time series (e.g., Albergel et al., 2008; Ford et al., 2014). The exponential filter approach has been extensively used in the literature and has been shown to perform well using in situ measurements as well as satellite SSM products (Albergel et al., 2008; Ceballos et al., 2005; Ford et al., 2014; González-Zamora et al., 2016; Pablos et al., 2018; Pasik et al., 2023; Paulik et al., 2014; Tian et al., 2022; Tobin et al., 2017; Wang et al., 2017; Yang et al., 2022; Zhao et al., 2008). However, all these RZSM products suffer from coarse spatial resolution due to the low coarse spatial resolution of the used SSM products (e.g., ERS, ASCAT, SMOS and SMAP). This data may be suitable for global applications, but not for applications requiring the field scale, such as irrigation management where farmers irrigate with different schedules within the same coarse-scale pixel. This is more important where the fields are less than 1 hectare in size (23 % of fields worldwide and 50–53 % in Africa and Asia (Lesiv et al., 2019)).

Very high spatial resolution products are becoming available today thanks to the availability of SAR (Synthetic Aperture Radar) data or the disaggregation of coarse products (Ouaadi et al., 2024a). As coarse products are disaggregated using optical reflectances and land surface temperature, they are either given with low temporal resolution due to the resolution of current thermal satellites combined to the effect of clouds, or inaccurate due to the use of reflectances, which do not contain information on soil water content, or both. By contrast, the all-weather SAR data are collected at high spatial resolution and are provided free of charge every six days by ESA's Sentinel-1 A and B. Note that Sentinel-1B has been out of service since December 2021, but has been replaced by Sentinel-1 C since December 5, 2024 (ESA, 2024; European Commission, 2024). Since its launch, several studies have been carried out to retrieve SSM from Sentinel-1 using different approaches, typically based on radiative transfer models (e.g., Ayari et al., 2023; Bai et al., 2017; Huang et al., 2019; Ouaadi et al., 2020) and machine learning algorithms (e.g., El Hajj et al., 2017; Ezzahar et al., 2023; Paloscia et al., 2013; Ya'nan et al., 2024). The accuracy achieved with most approaches is in the range 0.05–0.06 m³/m³. This accuracy can drop when applied over large areas, mainly due to (i) the simplification or neglect of certain processes in retrieval approaches, (ii) the model parameter calibration or (iii) the sensor characteristics (e.g., a high angle of incidence is not optimal for estimating SSM). Overall, the estimated SSM is reasonable for annual crops such as wheat, maize and canopies with similar structure. Over trees, the estimation is still challenging because of the limited penetration of the C-band as well as the multilayer complex geometry. However, to date, SAR based approaches are the most accurate method to estimate SSM compared to optical or disaggregated approaches. Indeed, although intercomparison studies at very high spatial resolution are very rare, Ouaadi et al. (2024a) found that Sentinel-1 products perform better than disaggregated approaches.

In this study, the RZSM is estimated using SSM products derived from Sentinel-1 data, including the backscatter coefficient and interferometric coherence over annual crops. The next section, Section 2, shows the study area, the in situ measurements and the exponential filter approach. Section 3 presents the results of RZSM estimation using the daily in situ SSM measurements, the 6-day Sentinel-1 SSM products compared to the 6-day in situ measurements, and the spatial pattern of the estimated RZSM. Section 4 is devoted to discussion and Section 5 to conclusions and some perspectives.

2. Data and methods

2.1. Study area

The soil moisture profiles used in this study are collected from 12 fields located at two sites, one in Morocco and the other in Spain (Fig. 1). The Moroccan site is located in the Haouz plain, in the center of Morocco (Fig. 1). The climate of the plain is a semi-arid Mediterranean climate, characterized by hot summers when temperatures can reach up to 45°C in July, and August and cold winters when temperatures can fall below 0°C in January. The reference evapotranspiration is 1600 mm/year, which far exceeds the average annual rainfall of 250 mm (Jarlan et al., 2016). Note that this average has dropped in recent years, a particularly marked period of drought in the country (between 70 mm/year and 190 mm/year since 2017). The soil texture is loamy-clay for F1, F2, F3, F4 and F5, while it is mainly clay for F6 and F7 (Table 1). The monitored fields are drip-irrigated and rainfed winter wheat fields. More details on the fields are summarized in Table 1.

The Spanish site is located in Catalonia region (Fig. 1). The climate is semi-arid Mediterranean influenced by a continental climate. This is resulting in hot summers against mild winters. The annual reference evapotranspiration is about 1100 mm/year. Most of the precipitation is occurred during autumn and spring with an annual precipitation

average of about 350 mm (Paolini et al., 2022). The five monitored fields are located in an irrigated district where the irrigation is ensured by the flood technique via the Urgell canal. The soil texture of the fields is loamy to silty-loam. More details about the fields are provided in Table 1.

2.2. Soil moisture database

2.2.1. In situ measurements

The soil moisture, including SSM and RZSM are measured using TDR sensors (Campbell Scientific CS616) on Moroccan fields. Data are collected every 30 min during the wheat agricultural season (Table 1). The sensors are installed at different depths between 5 and 35 cm. For F1-F5, the average value of two sensors installed one under and the other between the drippers (at 5 cm depth) is considered as representative of the field. The RZSM sensors are installed at 15, 25 and 35 cm depth for F1 and F2; 15 and 30 cm for F3, F4 and F5; 10 and 15 cm for F6 and F7. It is worth mentioning that the monitored root zone in this study (10–35 cm) is the zone that contains most of the roots of annual crops (Ali et al., 2019; Ehdaie et al., 2010; Fan et al., 2016; Fang et al., 2021; Hodgkinson et al., 2017; Y. Li et al., 2021; Mawodza et al., 2020). The sensors are calibrated using the gravimetric technique. More details on the database are available in Ouaadi et al. (2021a).

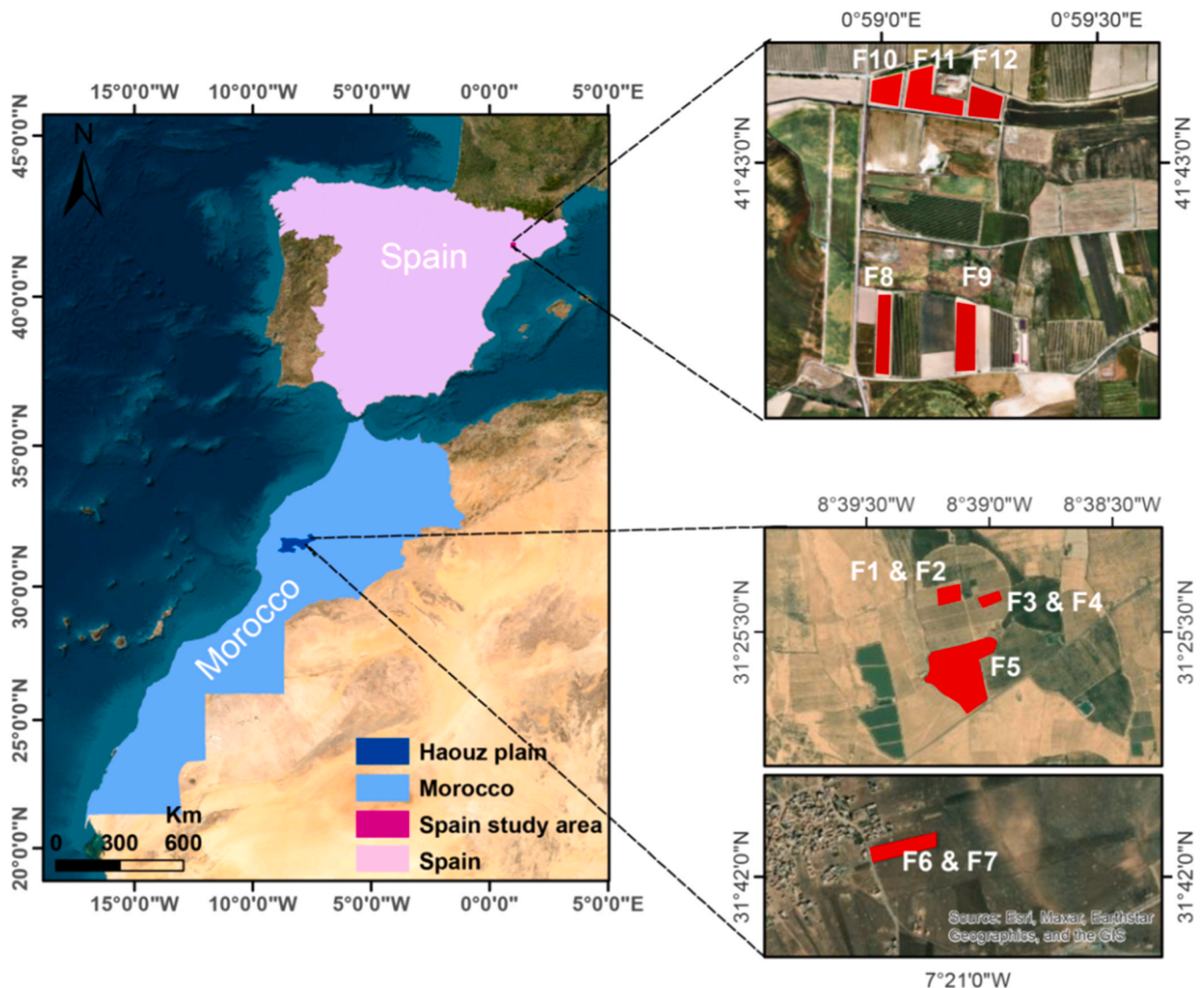


Fig. 1. Location of the studied fields (right maps) in both sites in Morocco and Spain (left map).

Table 1
General information about the twelve monitored fields. Clay and sand percentages for F8-F12 are not available.

Season	F1 Nov 2016–May 2017	F2 Nov 2017–June 2018	F3 Nov 2016–May 2017	F4 Nov 2017–June 2018	F5 Jany –June 2019	F6 Dec 2016–June 2017	F7 Nov 2017–May 2018	F8 May–July 2021	F9 May–Sept 2021	F10 May–Sept 2021	F11 May–Aug 2021	F12 May–Sept 2021
Crop	Wheat	Wheat	Wheat	Wheat	Wheat	Wheat	Wheat	Maize	Maize	Maize	Maize	Maize
Irrigation	Drip	Drip	Drip	Drip	Drip	Rainfed	Rainfed	Flood	Flood	Flood	Flood	Flood
Area (ha)	1.5	1.5	1.5	1.5	12	1	1	1	1.3	0.8	1.5	0.9
Clay (%)	37.5	37.5	37.5	37.5	37.5	47.5	47.5	18.5	18.5	18.5	18.5	18.5
Sand (%)	32.5	32.5	32.5	32.5	32.5	18.5	18.5	18.5	18.5	18.5	18.5	18.5
Soil texture classifications	Loamy-clay	Loamy-clay	Loamy-clay	Loamy-clay	Loamy-clay	Clay	Clay	Loam	Loam	Silty-loam	Silty-loam	Silty-loam

For the Spanish site, soil moisture is measured using a low-cost network composed of sensors connected to a data logger called LoNIM (Low-cost Network for Environmental Monitoring). The system is designed at CESBIO (<http://www.cesbio.cnrs.fr/>) and is allowing hourly automatic measurements (see Ouaadi et al. 2024a for more details). This database was collected as part of the LIAISE project (Boone et al., 2025). For each field, two sensors are buried one at 5 cm and one at 20 cm depth. The five fields are cropped and monitored during summer (see Table 1). The data are calibrated using measurements from a station located close to the studied fields (Ouaadi et al., 2024a).

2.2.2. Satellite surface soil moisture product

The SSM product used in this study is derived from Sentinel-1 data, including the backscattering coefficient (20 m resolution) and the interferometric coherence (50 m resolution). The algorithm is based on the use of a simplified radiative transfer model (backscattering model) in an inverse scheme using a “brute-force” algorithm to retrieve SSM with a 50 m resolution. The radiative transfer model used is the water cloud model (WCM, Attema and Ulaby 1978), accounting for the backscattering contribution from the vegetation, coupled to Oh model (Oh et al., 1992), accounting for the soil backscattering contribution, to the canopy total backscattering measured by the satellite. The interferometric coherence is used to estimate the above-ground biomass used as vegetation descriptor in the WCM. Details about the algorithm used to retrieve SSM can be found in Ouaadi et al., 2020. The soil roughness, represented by the root mean square height $-h_{rms}$ in the Oh model, is retrieved conjointly with SSM by exploring the range from 0 to $0.5 \text{ m}^3/\text{m}^3$ for SSM and from 0.1 cm to 1.5 cm for h_{rms} . Note that these ranges are determined based on field observations and the literature reported values. Also, the h_{rms} is considered constant thought the season as there is no soil tilling after the sowing (Ouaadi et al., 2020, 2021a). The SSM product was evaluated over Morocco, Tunisia (Ouaadi et al., 2020) and Spain (Ouaadi et al., 2024a) and used for irrigation and evapotranspiration mapping (Ait Hssaine et al., 2021; Laluet et al., 2024; Ouaadi et al., 2021b).

2.3. Rainfall and irrigation

The rainfall is collected using automatic weather stations installed near the fields for the Moroccan site. The rainfall measurements are collected at 30-min time step and summed on a daily basis. For the Spanish fields, the rainfall data are obtained from a nearby weather station, the Tornabous station, made available by the Ruralcat digital platform (<https://ruralcat.gencat.cat/agrometeo.estacions>).

The irrigation timing and amounts are available for F1-F4, while for F5 and F8-F12, the timing is determined by the analysis of SSM increases, and an approximate value of 10 mm and 50 mm is adopted for F5 (drip irrigation) and F8-F12 (flood irrigation), respectively. These are approximate values which are typically the average given per event for each irrigation technique and are accepted for the purpose of this study as irrigation is only required to show the occurrence of irrigation for the analysis of the RZSM time series.

2.4. Exponential filter

The Exponential model is a semi-empirical model that was introduced by Wagner et al. (1999) and modified later on by Albergel et al. (2008). Wagner et al. (1999) have proposed linking soil moisture in the root zone to that at the surface by the mean of an exponential filter. This approach is based on a water balance model simulating the soil in two layers. The first is the surface layer that interacts with the external environment. The soil moisture in the surface layer is the surface soil moisture that can be estimated from remote sensing data. The second layer is the root zone, which only exchanges with the surface layer. This layer is regarded as a reservoir, with the flow of water exchanged with the surface layer being proportional to their difference in soil moisture.

The water balance can therefore be expressed as follows:

$$L \frac{d\theta_r(t)}{dt} = C(\theta_s(t) - \theta_r(t)) \quad (1)$$

Where θ_r and θ_s are root and surface soil moisture, respectively. L is the root zone layer depth, t is the time and C is the pseudodiffusivity constant. By setting $T = L/C$, the solution of Equ. 1 is as follows:

$$\theta_r(t) = \frac{1}{T} \int_{-\infty}^t \theta_s(\tau) e^{-(t-\tau)/T} d\tau \quad (2)$$

T is a time parameter expressed in days. It characterizes the temporal variation of soil moisture. Although several important processes that have an impact on the water fluxes exchange are not taken into account in this simple model, including plant water uptake (transpiration) and the hydraulic properties of the soil, [Albergel et al. \(2008\)](#) have reported that T can be considered as a parameter that accounts for these processes. Consequently, different optimum values of T are found in the literature, depending on crops, climate, soil types and depths. In this study, the sensitivity of the approach to the optimum T value is investigated by exploiting a range of T values between 1 and 40 following [Albergel et al. \(2008\)](#), [Ford et al. \(2014\)](#) and [Tobin et al. \(2017\)](#) (Section 3.1.1).

In order to use regular observations provided by time intervals, the discrete form of Equ. 3 is useful for practical uses. [Wagner et al. \(1999\)](#) defined a soil water index (SWI), varying between 0 and 1, based on the discrete solution:

$$SWI(t_N) = \frac{\sum_{t=1}^N SSM(t_i) e^{-(t_N-t_i)/T}}{\sum_{t=1}^N e^{-(t_N-t_i)/T}} \quad (3)$$

SSM is the discrete measurements of θ_s obtained by the satellites. The frequency of its availability can vary according to the revisit time of the satellite, from 1 day for coarse products such as SMOS to 6-day with the very high resolution SAR Sentinel-1 (and even more). Note that in the calculus of SWI, SSM is rescaled also between 0 and 1. In this study, the soil moisture at wilting point (θ_{wp}) and at field capacity (θ_{fc}) are used to rescale SSM. Similarly, θ_{wp} and θ_{fc} are used to obtain RZSM from SWI. It is worth pointing out that [Wagner et al. \(1999\)](#) have used θ_{wp} and the mean of θ_{fc} and the total water capacity in the original approach. The authors, however, also proposed and evaluated other alternatives, among which θ_{wp} and θ_{fc} (used in this study) have proved the best performance.

Later on, [Albergel et al. \(2008\)](#) have proposed a recursive formulation of Equ. 3:

$$SWI_N = SWI_{N-1} + K_N(SSM(t_N) - SWI_{N-1}) \quad (4)$$

where SWI_{N-1} is the predicted SWI at t_{N-1} ; the last time an observation of SSM was available. K_N is between 0 and 1, and is expressed as follows:

$$K_N = \frac{K_{N-1}}{K_{N-1} + e^{-(t_N-t_{N-1})/T}} \quad (5)$$

This recursive formula makes it easier to manage predictions in the presence of gaps in the input SSM data. In other words, the estimation of a SWI at time t_N is requiring the last predicted SWI and K_N at time t_{N-1} and the SSM observation at time t_N . For the first estimation, the approach is initiated with $K_1 = 1$ and $SWI_1 = SSM(t_1)$. Finally, the estimated RZSM is obtained as follows:

$$RZSM_N = SWI_N * (\theta_{fc} - \theta_{wp}) + \theta_{wp} \quad (6)$$

3. Results

This section consists of three parts. First, the results using daily in situ data are evaluated in order to assess the effect of data availability on the estimation, investigate the sensitivity for T and analyze the time series and scatterplots. Next, the estimation of RZSM using Sentinel-1

SSM product with a 6-day time step is evaluated by comparison with a 6-day in situ measurement. Finally, the spatial pattern of RZSM is analyzed using maps derived over the Spanish study site.

3.1. Daily estimation

3.1.1. RZSM sensitivity to T and measurements depth

Using daily SSM measurements from the studied fields at 10–20 cm depth, [Fig. 2](#) shows the variation of the correlation coefficient (R), the root mean square error (RMSE) and the bias computed between the estimated and the measured RZSM for T ranging from 1 to 40 with a time step of 5 days. [Fig. 2](#) illustrates a marked decrease in the performance of the approach with increasing T, in particular degradation in R and RMSE. Overall, the best results are obtained for $T = 1$ to $T = 5$ days for all the fields separately and using the entire database ([Fig. 3](#)), with an average R value of 0.85, RMSE of $0.06 \text{ m}^3/\text{m}^3$ and bias = $0.03 \text{ m}^3/\text{m}^3$. The increase in T implies a smoothing or damping of soil moisture peaks, leading to an underestimation of high values in RZSM estimations (as shown in [Fig. 3](#)).

If the fields are observed separately ([Figs. 2](#)), 58.3% of the fields show reasonable metrics for the entire T range, with degradation limited to 33.6 % in R for instance. In contrast, 41.4 % of fields (F8, F10, F12, F11 and F3) exhibit a 78.7 % decline in the R value if F3 is excluded (~100 % decline if F3 is included). F3 performed quite differently to the other fields, showing a complete drop from 0.64 ($T = 1$ day) to 0 ($T = 35$ days). RMSE follows approximately the same trend as R. Same fields with decreased R values also show a strong degradation of RMSE. For example, the highest RMSE values are observed for F10, F11 and F12 (values between $0.09 \text{ m}^3/\text{m}^3$ and $0.15 \text{ m}^3/\text{m}^3$; increasing overall with T). Interestingly, the RMSE of F3 and F8 is reasonable and its variation is limited between $0.03 \text{ m}^3/\text{m}^3$ and $0.05 \text{ m}^3/\text{m}^3$. Similarly, the bias is high for fields with high RMSE values but is more stable with variation of T value. Note that the RZSM measurement depth used here for fields F8–F12 is 20 cm, while the measurements for all the other fields are between 10 and 15 cm, which may partly explain the observed differences in performance.

In order to investigate the impact of measurement depth on the metrics and the optimum T value, [Table 2](#) summarizes the statistical metrics obtained for the 20–35 cm zone for 5 fields for which different measurement depths are available (see [Section 2.2.1](#)).

The results show a decrease in R and an increase in RMSE with increasing measurement depth, while the bias is fairly stable. In particular, the maximum mean R value for the five fields at a depth of 30–35 cm is 0.72, which is 12 % less than the maximum mean R value ($R = 0.82$) for the same fields at 10–15 cm depth. Note that this maximum value is obtained for higher T values ($T \geq 15$ days) at depths of 30–35 cm compared with depths of 10–15 cm (optimum $T = 1$ –5 days). For these T values, considered optimal for R, RMSE and bias reach also the lowest values (RMSE = $0.038 \text{ m}^3/\text{m}^3$ and $0.044 \text{ m}^3/\text{m}^3$ and bias = $-0.002 \text{ m}^3/\text{m}^3$ and $-0.022 \text{ m}^3/\text{m}^3$ for 10–15 cm and 30–35 cm depth, respectively). Interesting enough, for F1 and F2, where measurements are available at 15, 25 and 35 cm depth, statistical metrics at 25 cm are slightly lower than those at 15 cm and higher than those at 35 cm.

It's also important to note that the fields are different in terms of irrigation technique, soil texture and vegetation type. These factors have an impact on infiltration and the distribution of soil moisture between the surface and the root zone, and therefore on the performance of the exponential filter.

3.1.2. Time series analysis of the estimated RZSM

[Fig. 4](#) shows the time series of estimated and observed RZSM at a depth of 10–20 cm depth for all fields for $T = 1$ day. Rainfall and irrigation amounts are also superimposed.

The overall seasonality and RZSM peaks are well produced for the majority of the fields, which accounts for the good statistical metrics reported in [Section 3.1.1](#). However, some false peak predictions are also

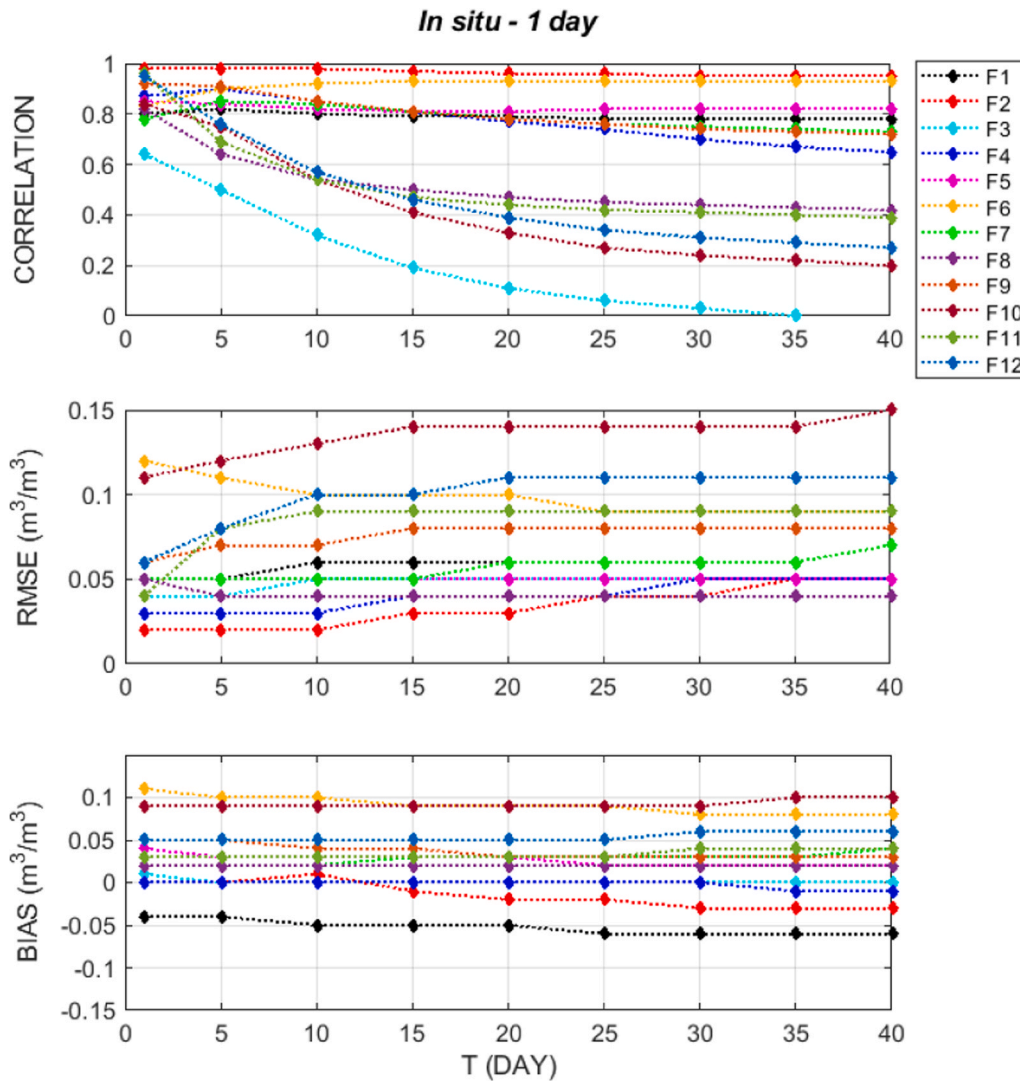


Fig. 2. Variation of R, RMSE and bias computed between the daily estimated and observed RZSM at 10–20 cm depth for T values ranging between 1 and 40 over all the studied fields.

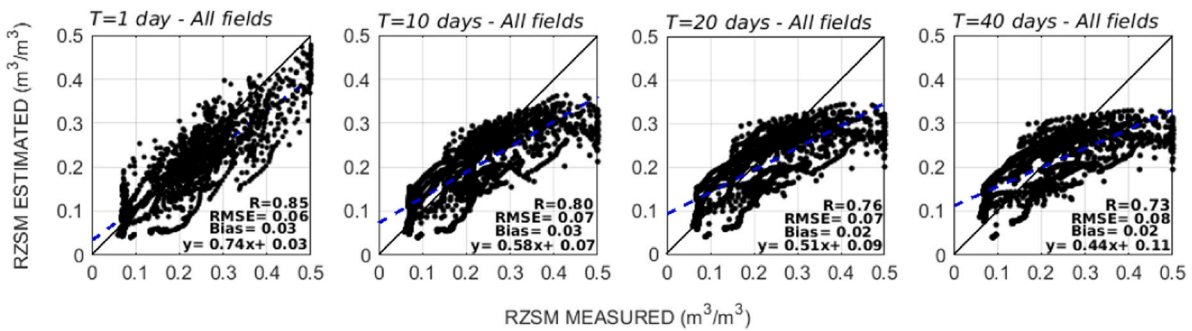


Fig. 3. Scatterplots between observed and estimated RZSM at 10–20 cm depth for four T values: 1 day, 10, 20 and 40 days using the entire database from all the fields.

noted, such as those observed between 20 March and 29 April in F1. This is related to SSM fluctuation in response to small rainfall events. Examples include the rain event on 29 April in F1 and F3 (2016–2017 agricultural season) and the two small rain events on 10 and 24 April in F2 and F4 (2017–2018 agricultural season). These small amounts of water have an impact on the surface but are not filtered to the root zone, mainly because they evaporate quickly from the surface given the high

temperatures in the region at this time of year. This could also explain the fluctuation in RZSM predictions in response to irrigation events between 20 March and 29 April; in particular that the irrigation technique is drip and the percentage of clay is high. Obviously, the fluctuations are most marked for low values of T (1 and 5 days), while the high T values smooth out the fluctuations, as already mentioned (Fig. 3). Fig. A1 in the appendix shows an example of F1 time series for T = 1, 10,

Table 2
Statistical metrics computed between the measured and estimated RZSM at daily basis at 25–35 cm depth for T ranging between 1 and 40 days.

		25 cm depth		30–35 cm depth				
		F1	F2	F1	F2	F3	F4	F5
T = 1	R	0.73	0.98	0.63	0.97	0.2	0.76	0.88
	RMSE (m ³ /m ³)	0.04	0.02	0.05	0.02	0.08	0.05	0.03
	bias (m ³ /m ³)	-0.02	0.01	-0.03	0.01	-0.04	-0.01	0.02
T = 5	R	0.79	0.98	0.7	0.98	0.08	0.85	0.9
	RMSE (m ³ /m ³)	0.04	0.02	0.05	0.03	0.08	0.04	0.03
	bias (m ³ /m ³)	-0.02	0	-0.04	0	-0.04	-0.01	0.02
T = 10	R	0.79	0.98	0.73	0.98	0.08	0.82	0.86
	RMSE (m ³ /m ³)	0.04	0.02	0.05	0.02	0.08	0.04	0.03
	bias (m ³ /m ³)	-0.02	-0.01	-0.04	-0.01	-0.04	-0.01	0.02
T = 15	R	0.79	0.97	0.74	0.98	0.2	0.82	0.84
	RMSE (m ³ /m ³)	0.04	0.03	0.05	0.02	0.09	0.04	0.02
	bias (m ³ /m ³)	-0.03	-0.01	-0.04	-0.01	-0.04	-0.01	-0.01
T = 20	R	0.78	0.96	0.74	0.97	0.27	0.8	0.83
	RMSE (m ³ /m ³)	0.04	0.03	0.05	0.04	0.09	0.04	0.03
	bias (m ³ /m ³)	-0.03	-0.02	-0.05	-0.02	-0.05	-0.01	0.01
T = 25	R	0.78	0.96	0.74	0.97	0.32	0.77	0.82
	RMSE (m ³ /m ³)	0.04	0.04	0.05	0.03	0.09	0.04	0.03
	bias (m ³ /m ³)	-0.03	-0.02	-0.05	-0.02	-0.05	-0.01	0.01
T = 30	R	0.78	0.95	0.74	0.96	0.34	0.75	0.81
	RMSE (m ³ /m ³)	0.04	0.04	0.06	0.04	0.09	0.05	0.03
	bias (m ³ /m ³)	-0.03	-0.03	-0.05	-0.03	-0.05	-0.01	0.01
T = 35	R	0.78	0.95	0.75	0.96	0.36	0.73	0.81
	RMSE (m ³ /m ³)	0.04	0.05	0.06	0.04	0.09	0.05	0.04
	bias (m ³ /m ³)	-0.04	-0.03	-0.05	-0.03	-0.05	-0.01	0.01
T = 40	R	0.79	0.95	0.75	0.96	0.37	0.71	0.81
	RMSE (m ³ /m ³)	0.04	0.05	0.06	0.04	0.09	0.05	0.04
	bias (m ³ /m ³)	-0.04	-0.03	-0.05	-0.03	-0.05	-0.01	0.01

20 and 40 days. However, the high T values also dampen the true variations observed in the measurements.

The impact of the rainfall event of 29 April 2017 (3.8 mm) is not the same for the two fields F1 and F3: an increase of 0.007 m³/m³ for F1 compared with 0.23 m³/m³ for F3 after two days. In contrast, the event of 24 April 2018 has the same effect on F2 and F4 (increase of the same magnitude). Taking into account the different growing conditions of the fields, including the irrigation scheduling and amounts and density of seeds, it is difficult to comment on the difference in impact of this single event, which moreover occurs at the end of the season when irrigation is stopped. At this time; the end of the winter season (May-June), the predictions are lower than the measurements. This could be related to the low moisture level in the surface layer (low SSM) due to high temperature values and the absence of watering events, while the high clay content of fields (F1-F7) maintains slightly high moisture in the deeper zone.

For some fields, the bias between estimates and measurements is constant throughout the season, as is the case for F1, or for specific periods such as the period from January to March on F5. Frequent watering events (irrigation or rainfall) may have led to continuous infiltration of water into the deep zone, which is retained by the high clay content. Indeed, the maximum bias and low mismatch in the reproduction of the trend and peaks are observed for F6 (2016–2017 agricultural season). First, the measurement level is higher than the estimation, which could be related to the moisture retention in the root zone (47.5 % clay). Second, the low fluctuation or variation in the measurement could be partly explained by the small amounts of rain that only impact the surface and then evaporate. This is supported by F7 being the next season of the same field (2017–2018), which shows a good match between the estimations and observations with a high level of RZSM (up to 0.4 m³/m³) as this season was wetter than 2016–2017.

For the summer fields (F8-F12), the estimated and measured RZSM are in good agreement in terms of tendency and amplitude, with the exception of F8. As the soil texture is loamy to silty-loam for these fields, and considering the time series of the other fields (F9-F12), this is unlikely caused by moisture retention in the root zone (different depth texture to surface texture). More likely, the problem lies with the

measurements considering the time series evolution as well.

3.2. 6-day Sentinel-1 and in situ measurements

In this section, the RZSM is estimated with a frequency of 6 days using Sentinel-1 SSM product and using 6-day in situ measurements for comparison purposes. Fig. 5 shows the obtained statistical metrics (R, RMSE and bias) as a function of T at 10–20 cm depth. Fig. A2 in the appendix is similar to Fig. 4 but using Sentinel-1 SSM product. Note that F3 and F4 are not evaluated for Sentinel-1 due to the specific growing conditions of these fields, which resulted in inaccurate SSM retrieval. For more details, the reader is referred to Ouaadi et al. (2020).

Overall, the results are similar between the daily measurements (Fig. 2) and the 6-day in situ measurements (Fig. 5). Using the Sentinel-1 SSM product, the scores are also reasonable but lower than those obtained using in situ measurements. For example, using all the data, a drop of around 26 % in terms of R is observed (0.81 using in situ measurements versus 0.6 using Sentinel-1 SSM product). Similarly, RMSE and bias increased: RMSE = 0.07 m³/m³ and bias = 0.03 m³/m³ using in situ measurements compared with RMSE = 0.12 m³/m³ and bias = 0.07 m³/m³ using Sentinel-1 product. This can be explained by the accuracy of the SSM product. Table 3 summarizes the results of the SSM estimation for all the fields. Indeed, Fig. 5 shows that the best results, with a correlation higher than 0.8, are obtained for F2 and F6, for which SSM is also estimated with good accuracy (Table 3). F5 also yields good statistical metrics with R > 0.7. Interestingly, the performance of the RZSM approach is low when T < 10 days for F1 and F7. Overall, the performance of all the Moroccan sites is the best for T = 10 days with different sensitivities to T in the range between 1 and 10 days. For instance, an improvement of 4.5 % in terms of R is observed for F1 while it is 41.2 % for F2. For RMSE, some fields show significant differences between T = 1 and T = 10 days (a decrease of 33 % for F7 for example), but as a whole, the best performance is obtained for T > 5 days and the bias is fairly constant throughout the T range. For the Spanish fields, a decrease in performance is observed with increasing T, with the exception of F9 which produces the lowest performance whatever the value of T (and a low SSM estimate as well, Table 3). In particular, the

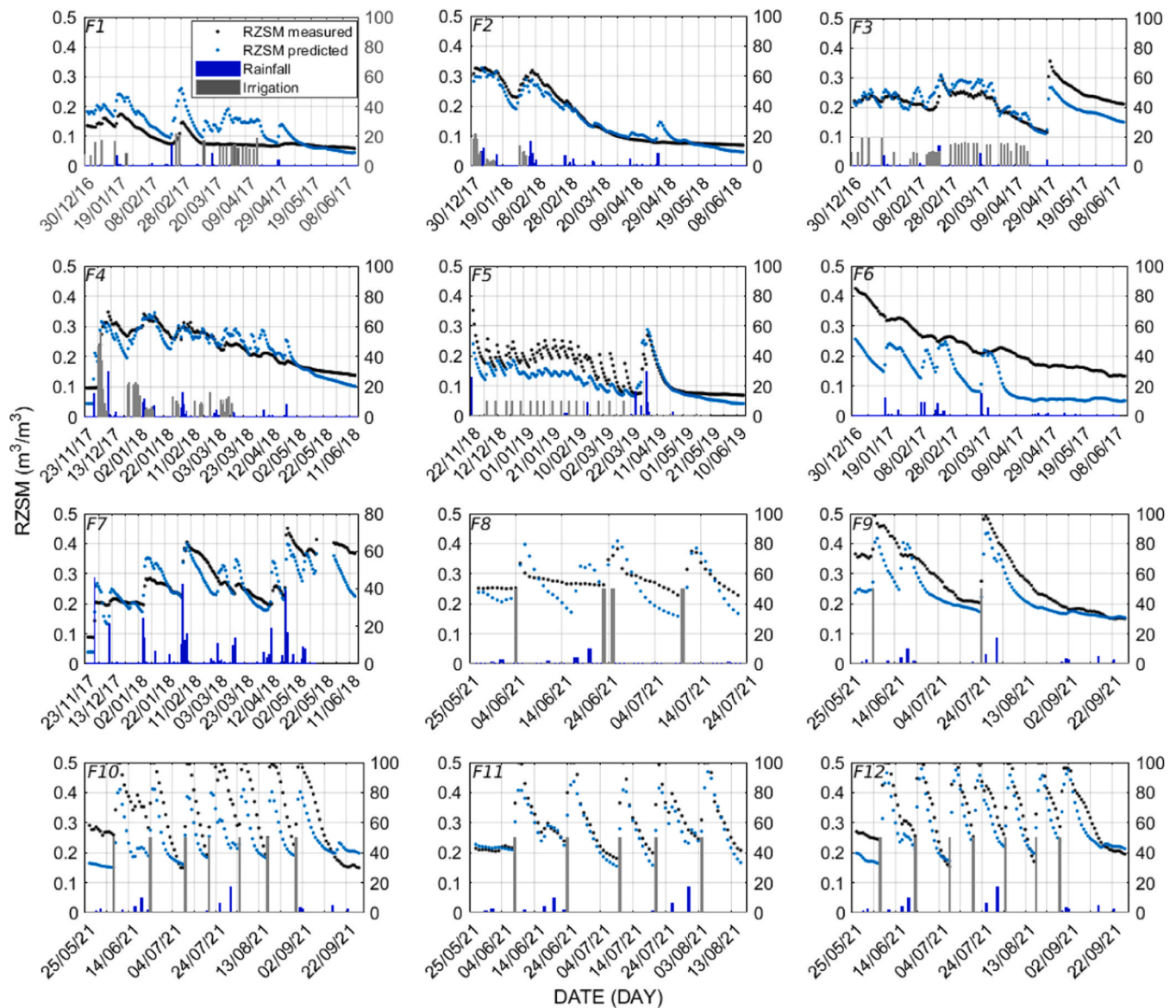


Fig. 4. Time series of the estimated and measured RZSM at 10–20 cm depth for all fields.

best R and RMSE are obtained for $T = 1$ day for all fields, while the bias is constant. This difference in the behavior of the RZSM estimation approach between the Spanish and Moroccan fields is mainly related to the difference in soil texture as already highlighted. The loamy to silty-loam soil in the Spanish site promotes rapid infiltration of water and does not retain much moisture over a long period, thus leading to a decline in the RZSM estimation with increasing T . This could also be accentuated by the type of crop (maize), which is characterized by tick roots that increase soil porosity.

For deeper RZSM, the results obtained using 6-day in situ measurements and Sentinel-1 product are presented in Table 4 and Table 5, respectively. As with daily in situ measurements, deeper layers require higher T values. For F1 and F2, for example, T values between 15 and 25 days are the best for a depth of 25 cm and between 20 and 30 days for a depth of 30–35 cm. This illustrates the importance of taking into account the infiltration time as a function of depth when estimating RZSM, as well as soil texture, which determines water retention.

3.3. Very high spatial resolution mapping of RZSM

Fig. 6 shows the RZSM maps estimated using the exponential filter

approach fed by Sentinel-1 SSM product over the study area in Spain for five selected dates in 2021. A crop classification map of 2021 and the corresponding NDVI maps calculated from Sentinel-2 are also presented for interpretation purposes. The crop map is obtained from the agricultural plot identification system of catalunia DUN-SIGPAC, which is available on the website (<https://agricultura.gencat.cat/ca/ambits/desenvolupament-rural/sigpac/mapa-cultius/>). Note that the shapefile of the crop map cadastre is used to extract only the agricultural area shown in the RZSM and NDVI maps.

The area is composed of an irrigated part to the west-north and a rainfed part to the east-south of the maps. This is best depicted by the NDVI maps, particularly in the July 2 map. Irrigation is provided by the old Urgel canal, which separates the irrigated from the rainfed part of the study area. The irrigated part is mainly composed of sweet fruit and cereals; winter crops followed by summer crops. The RZSM map of January 15 shows that the rainfed fields are dry in contrast to the irrigated part and the extreme south-east. This is most likely due to irrigation, as no rainfall event has been recorded since January 10. The extreme south-east part in the rainfed part is mainly cropped with olive groves and vineyards, which also supported by the high NDVI values of January 15 map. It could be irrigated using the new Segarra-Garrigues

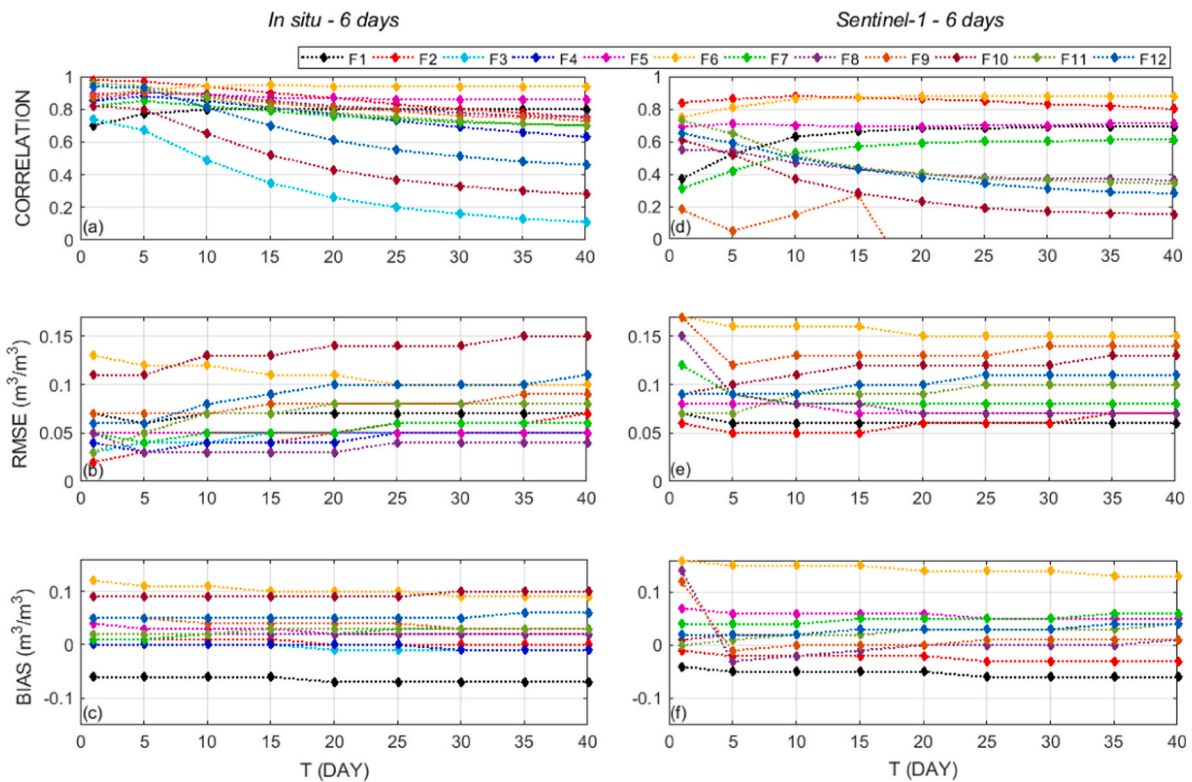


Fig. 5. Variation of the correlation coefficient, RMSE and bias computed between the 6-day estimated from Sentinel-1 and in situ SSM and observed RZSM for T values ranging between 1 and 40 over all the studied fields at 10–20 cm depth.

Table 3
Statistical metrics of the SSM estimated from Sentinel-1 for all the fields except F3 and F4 (see the text).

	F1	F2	F5	F6	F7	F8	F9	F10	F11	F12
R	0.64	0.84	0.8	0.82	0.59	0.57	0.53	0.73	0.8	0.74
RMSE (m ³ /m ³)	0.04	0.05	0.04	0.06	0.09	0.13	0.10	0.08	0.10	0.09
Bias (m ³ /m ³)	0.01	-0.02	0.03	0.04	0.03	-0.11	-0.06	0.03	-0.07	-0.06

canal which crosses the rainfed part near the extreme south-east (more information in Ouaadi et al. 2024a).

April 27, on the other hand, is wetter than January 15 and displays higher moisture variability. This variability in RZSM could be linked to the ~8 mm of rainfall recorded on April 26, distributed between 04 h and 14 h. Given the low temperatures (maximum of 13°C at 12 h), it's likely that the water had time to infiltrate into the root zone. The dry patch in the rainfed area, however, could be attributed to the fact that the area is non-irrigated and, as a result, the soil is drier than the irrigated part, which already contains a percentage of moisture. The effect of irrigation is again more pronounced in summer, as shown on the July 2 map. Some fields are dry but have been wetted in the September 12 map. This is probably an irrigation event, given that no rainfall event has been recorded after a 0.3 mm rainfall on September 9. This highlights the importance of very high spatial resolution for monitoring the spatial variability of moisture in agricultural regions. The summer NDVI shows a dominance of low values in the rainfed part, and thus of bare soils. However, RZSM is high in many fields. With the exception of a few irrigated fields in the extreme south and a few scattered fruit trees, the majority of fields are non-irrigated. The high RZSM values are due to the high SSM values retrieved in some specific areas. This is attributed to the potential subsurface scattering found in the region by previous studies. Further investigation of this phenomenon on the Sentinel-1 SSM product has been carried out in Ouaadi et al. (2024a). Finally, a homogeneous rainfall event is more likely to induce homogeneous soil wetting, as is the case with the October 30 RZSM map. The entire study area displays

high RZSM values after a 6 mm rainfall event by Sentinel-1 overpass at 06h30 with a maximum temperature of 14°C.

4. Discussion

The exponential filter method using Sentinel-1 SSM product is yielding encouraging results and, given its simplicity, this approach is extremely practical for large-scale, very high-resolution applications. However, this simplicity is mainly due to the use of one parameter (T) in addition to SSM data. T is assumed to contain all the information on texture, organic matter, evaporation, etc. On one hand, this is a major advantage, since only one parameter is required. On the other hand, enclosing all the impact of these processes in a single parameter makes it difficult to generalize over a large area with different conditions.

Overall, the performance of the approach is determined by the T-value and the accuracy of the SSM product. Indeed, using the entire in situ SSM database with a non-optimal T value can result in a decrease of up to 14 % in R and an increase of up to 25 % in RMSE (of RZSM estimation) compared to using the T optimal value. Inversely, for an optimal T value, an error of 6–10 % in the SSM data results in a decrease between 2.3 % and 5.8 % in R and an increase of 16.6 % in RMSE. Note that an SSM error of X % (e.g., X = 10) was generated by adding ± X % noise to the entire database of in situ SSM measurements. The results of this analysis show that T has a stronger impact on RZSM estimation than SSM accuracy. However, the field-by-field analysis highlights the variation in the impact weight of each factor by field, and it is therefore

Table 4

Statistical metrics computed between the observed and estimated RZSM using in situ SSM measurements with a 6-day frequency at 25–35 cm depth.

		25 cm depth		30–35 cm depth				
		F1	F2	F1	F2	F3	F4	F5
T = 1	R	0.65	0.96	0.59	0.95	0.49	0.8	0.9
	RMSE (m ³ /m ³)	0.05	0.03	0.06	0.03	0.08	0.04	0.03
	bias (m ³ /m ³)	-0.03	0.01	-0.05	0.01	-0.06	-0.01	0.02
T = 5	R	0.74	0.95	0.68	0.96	0.4	0.85	0.91
	RMSE (m ³ /m ³)	0.04	0.03	0.06	0.02	0.08	0.04	0.03
	bias (m ³ /m ³)	-0.03	0.01	-0.05	0.01	-0.06	-0.01	0.02
T = 10	R	0.79	0.91	0.77	0.95	0.21	0.85	0.87
	RMSE (m ³ /m ³)	0.04	0.04	0.06	0.03	0.09	0.04	0.03
	bias (m ³ /m ³)	-0.04	0.01	-0.05	0.01	-0.06	-0.01	0.02
T = 15	R	0.81	0.87	0.8	0.92	0.08	0.82	0.84
	RMSE (m ³ /m ³)	0.05	0.05	0.06	0.04	0.09	0.04	0.03
	bias (m ³ /m ³)	-0.04	0.01	-0.06	0	-0.06	-0.01	0.02
T = 20	R	0.82	0.83	0.82	0.89	0.01	0.79	0.81
	RMSE (m ³ /m ³)	0.05	0.06	0.06	0.04	0.09	0.04	0.03
	bias (m ³ /m ³)	-0.04	0.01	-0.06	0	-0.06	-0.01	0.01
T = 25	R	0.82	0.79	0.83	0.85	-0.06	0.76	0.79
	RMSE (m ³ /m ³)	0.05	0.06	0.06	0.05	0.09	0.04	0.03
	bias (m ³ /m ³)	-0.04	0.01	-0.06	0	-0.06	-0.01	0.01
T = 30	R	0.83	0.76	0.83	0.82	-0.1	0.73	0.77
	RMSE (m ³ /m ³)	0.05	0.06	0.07	0.05	0.09	0.05	0.03
	bias (m ³ /m ³)	-0.05	0	-0.06	0	-0.06	-0.01	0.01
T = 35	R	0.83	0.73	0.84	0.8	-0.12	0.7	0.76
	RMSE (m ³ /m ³)	0.05	0.07	0.07	0.05	0.09	0.05	0.03
	bias (m ³ /m ³)	-0.05	0	-0.06	0	-0.06	-0.01	0.01
T = 40	R	0.83	0.7	0.84	0.77	-0.14	0.68	0.75
	RMSE (m ³ /m ³)	0.05	0.07	0.07	0.06	0.09	0.05	0.03
	bias (m ³ /m ³)	-0.05	0	-0.07	0	-0.06	-0.01	0.01

Table 5

Statistical metrics computed between the observed and estimated RZSM using Sentinel-1 SSM products with a 6-day frequency at 25–35 cm depth.

		25 cm		30–35 cm		
		F1	F2	F1	F2	F5
T = 1	R	0.36	0.85	0.38	0.84	0.65
	RMSE (m ³ /m ³)	0.06	0.05	0.06	0.05	0.07
	bias (m ³ /m ³)	-0.02	-0.01	-0.04	-0.02	0.06
T = 5	R	0.5	0.87	0.5	0.88	0.66
	RMSE (m ³ /m ³)	0.5	0.05	0.05	0.05	0.07
	bias (m ³ /m ³)	0.05	-0.01	-0.04	-0.02	0.05
T = 10	R	0.62	0.87	0.61	0.9	0.59
	RMSE (m ³ /m ³)	0.04	0.05	0.05	0.04	0.06
	bias (m ³ /m ³)	-0.02	-0.01	-0.04	-0.02	0.05
T = 15	R	0.66	0.86	0.64	0.9	0.54
	RMSE (m ³ /m ³)	0.04	0.05	0.05	0.05	0.06
	bias (m ³ /m ³)	-0.03	-0.02	-0.04	-0.02	0.05
T = 20	R	0.68	0.85	0.66	0.89	0.51
	RMSE (m ³ /m ³)	0.04	0.06	0.05	0.05	0.06
	bias (m ³ /m ³)	-0.03	-0.02	-0.05	-0.03	0.05
T = 25	R	0.69	0.83	0.67	0.88	0.49
	RMSE (m ³ /m ³)	0.04	0.06	0.05	0.05	0.06
	bias (m ³ /m ³)	-0.03	-0.02	-0.05	-0.03	0.05
T = 30	R	0.69	0.81	0.68	0.86	0.48
	RMSE (m ³ /m ³)	0.04	0.07	0.05	0.06	0.06
	bias (m ³ /m ³)	-0.03	-0.02	-0.05	-0.03	0.04
T = 35	R	0.7	0.79	0.68	0.85	0.48
	RMSE (m ³ /m ³)	0.04	0.07	0.06	0.06	0.06
	bias (m ³ /m ³)	-0.03	-0.03	-0.05	-0.03	0.04
T = 40	R	0.7	0.77	0.68	0.83	0.47
	RMSE (m ³ /m ³)	0.05	0.07	0.06	0.06	0.06
	bias (m ³ /m ³)	-0.03	-0.03	-0.05	-0.03	0.04

recommended to consider both in the improvement of the RZSM approach.

4.1. The T parameter

T is highly dependent on soil depth and texture (Ceballos et al., 2005; De Lange et al., 2008; Wang et al., 2017). Indeed, the soil texture is

impacting the size and connectivity of soil pores, and hence impacting the trajectory and speed of water transfer from the surface to the root zone. For example, loamy soils contain more and larger pores than clay soils. In addition, larger pores favor the development of more fines roots (Xu et al., 2020). This is observed in this study, where the increase in T has led to a drop in approach performance at the Spanish site (loamy to sandy-loam soil), using in situ SSM or Sentinel-1 product. Using a 1-D vadose zone model to study the impact of soil texture, De Lange et al. (2008) found that the best T for clay soils is lower than for sandy soils. This is the opposite of what we found in this study. One explanation is that sandy soils favor rapid infiltration, unlike clay, whose high capillarity ensures strong water retention in the smallest pores (Baldwin et al., 2017; Vereecken et al., 1989). This is supported by the results of Wang et al. (2017), who found a negative correlation between T and sand fraction compared to a positive correlation with clay fraction. The capacity of sandy soils to retain water is low due to their higher hydraulic conductivity. This results in a strong temporal relationship between surface and root zone moisture, as was observed for the Spanish fields using in situ measurements or Sentinel-1 product. It is important to note, however, that other studies have shown a limited impact of soil texture on T. For instance, Wang et al. (2017) found that texture is impacting T for deeper soils (at 50 cm compared to 25 cm) and explained this by the limited impact of surface process on RZSM for deeper layers. Albergel et al. (2008) also highlighted a limited impact of soil texture on T using model simulations with SAFRAN-ISBA-MODCOU. It is worth noting that other soil properties, including bulk density, organic matter content and pedality, also have an impact on the infiltration process (Maraseni and Pandey, 2014; Prasad et al., 2018) and, consequently, on T and RZSM. It is therefore likely that soil texture is combined with other soil properties and even other factors (e.g. climate) that have an impact on T.

The optimum T value found in this study is 1 for the Spanish site and between 5 and 10 for the Moroccan site at 15–20 cm depth. These values fall within the range reported by some previous studies (e.g., Albergel et al., 2008; Ford et al., 2014; Yang et al., 2022) while they are lower than those obtained in others (e.g., Ceballos et al., 2005; Wagner et al., 1999). This could be associated to the combined effect of all the factors

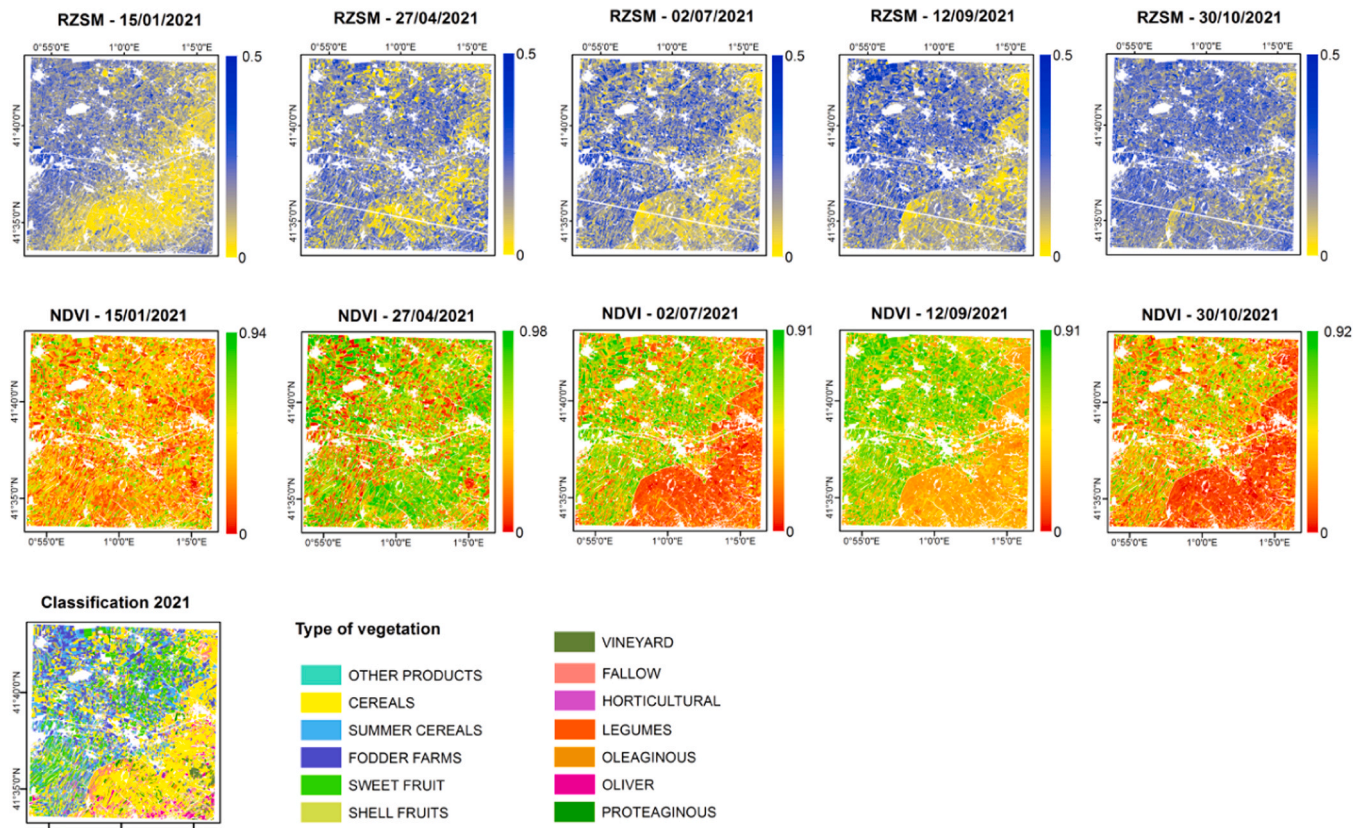


Fig. 6. Maps of the estimated RZSM using the exponential filter, Sentinel-2 NDVI and the crop map obtained from DUN-SIGPAC over the Spanish study area for 2021. The white spots corresponds to non agricultural area.

affecting the approach (e.g. soil type, climate, SSM ...). For example, the semi-arid climate of the Moroccan and Spanish sites is characterized by a high evaporation demand, which could partly explain the low optimum T values found in this study. By contrast, all studies, including this one, have shown that the optimum value of T increases with depth (Albergel et al., 2008; Ceballos et al., 2005; Wang et al., 2017). The optimum T value in this study is 15–25 days for 25 cm depth and 20–30 days for 30–35 cm depth. Indeed, high values of T mean more time for infiltration and a smoother variation of RZSM as soil moisture is more stable over time in deeper zones (Guber et al., 2008; Wang et al., 2017). However, the performance of the approach declines with depth due to the associated increasing decoupling between SSM and RZSM (Guber et al., 2008; Martínez-Fernández and Ceballos, 2003; Wang et al., 2017).

Previous studies have shown a seasonal variation in T, mainly attributed to climatic conditions (Albergel et al., 2008). Indeed, the results of this study show a difference in performance between two successive seasons for the same field with the same crop and irrigation technique. The 2017–2018 agricultural season (fields monitored: F2 and F4) was wetter than the 2016–2017 season (F1 and F3). For instance, the RZSM statistical metrics on F1 are lower than on F2 (the same field but monitored during two different seasons). In particular, the optimal T is over 10 days for F1, while the metrics are fairly stable for T between 1 and 10 days for F2, using either 6-day in situ measurements or Sentinel-1 SSM product. This is in agreement with previous studies which have reported more accurate RZSM predictions in sites that receive more rainfall (Ford et al., 2014; Mahmood et al., 2012). Similar conclusions can be drawn for F3 and F4, but one must be cautious in interpreting this field as it has been shown that its specific growth conditions have a particular impact on the estimation and measurement of the various processes (Ouaadi et al., 2020, 2023).

The large-scale transferability of the RZSM approach is subject to T. Although it is possible to calibrate it by field for an area of interest, the

variation over the years in response to climate (e.g., amount of rainfall, temperature) makes the task of ongoing applicability challenging. In other words, T calibration by soil and vegetation can be carried out one year and applied in subsequent years if its seasonal variation is negligible. An interesting method, envisaged as an extension of this work, is the integration of the different factors impacting the performance of the approach in the determination of the optimal T value. This can be achieved by estimating T using machine learning fed by vegetation indices, climatic variables and soil properties such as its texture. The application of the approach on a large scale requires maps of the wilting point and field capacity. Such maps can be derived from a piecewise model which is allowing extracting field capacity and wilting point as transition points between different hydrologic regimes (Dong et al., 2023; Akbar et al., 2018). It is also important to test the approach on a large SSM database for different climates, soils, vegetation types, irrigation techniques and using other very high spatial resolution SSM products.

4.2. The SSM product accuracy

Very high spatial resolution SSM product is used in this study. The growing number of such approaches in recent years (Ouaadi et al., 2024a) is encouraging for RZSM mapping at very high spatial resolution, and this study is a first step towards this objective. Indeed, the retrieved RZSM maps have illustrated the spatial variability of RZSM between adjacent fields. This variability cannot be depicted using the coarse resolution products always used in literature (Liu et al., 2024). SAR-derived products are the most accurate at very high spatial resolution (Ouaadi et al., 2024a) thanks to the unique very high spatial resolution of SAR sensors combined with adequate temporal frequency (Li et al., 2021; Moran et al., 2004). However, the results revealed the clear impact of SSM product quality on RZSM estimation where the

inaccuracies in SSM are propagated to RZSM, as in the case of F8 for example. To improve the product quality, both the data and the approach used to retrieve it must be improved. The SSM product used in this study is based on Sentinel-1 data collected in the C-band (wavelength around 6 cm). The penetration of this wavelength in the canopy is moderate and the backscattered energy is a mixture of soil and vegetation contributions (Ulaby et al., 1996). The use of upcoming missions with larger wavelengths has the potential to improve decoupling the volume (or vegetation) from soil contribution, as well as better penetration into the soil to minimize SSM estimation errors (Das and Kumar, 2015; Lal et al., 2023). This is expected to be achieved in the very near future with the launch of the Rose-L (Lannini et al., 2024) and NISAR (NISAR, 2019) L-band missions, and the Biomass P-band mission (CEOS, 2024, Qeegan et al., 2019). These data could be useful to better understand some of the specific effects observed at C-band, such as subsurface scattering (Lal et al., 2023). Also, the water cloud model used to estimate SSM is a simple single-layer approach with two coefficients to be calibrated per crop type. While its simplicity is preferable for inversion purposes, an improvement of coefficients optimization and representation of the canopy and its water and geometry characteristics is also likely to improve the estimations. Some specific phenomena neglected in the modeling of canopy response may contribute significantly to the total response measured by the satellite. Subsurface scattering is assumed to induce false high SSM values, as observed in RZSM maps. Indeed, Wagner et al. (2022) have underlined the need to include the subsurface scattering component to minimize errors in the SSM retrieval from active microwave data. Similarly, water droplets on the canopy surface (dew and water interception) are neglected, even though they have an impact on backscattered intensity (Riedel et al., 2002; Ulaby et al., 1986) and interferometric coherence (Ouaadi et al., 2024b). Finally, changes in canopy geometry during the season must also be taken into account; the appearance of wheat (and eventually maize) heads, for example, induces an increase in signal intensity (Ouaadi et al., 2020; Picard et al., 2003). Its contribution must be added to the volume contribution from the vegetation (Ulaby et al., 1986).

5. Conclusion

The aim of this study is to estimate RZSM at very high spatial resolution using the exponential filter and Sentinel-1 SSM product at 50 m spatial resolution. First, daily in situ measurements are used to investigate the sensitivity of the estimation to the time parameter T. Then, 6-day Sentinel-1 products are used to retrieve and map RZSM. Statistical measurements show encouraging results with R, RMSE and bias of 0.6,

0.12 m³/m³ and 0.07 m³/m³ using Sentinel-1 SSM products from the entire database covering twelve fields in Morocco and Spain. Obviously, the results are lower than those obtained using in situ measurements (R = 0.81, RMSE = 0.07 m³/m³ and bias = 0.03 m³/m³). This is mainly attributable to the SSM product quality, where the accuracy of RZSM per field varies according to the variation in the SSM accuracy. The field-by-field analysis highlighted the sensitivity of the RZSM approach to the T parameter. The optimum value of T is found to be impacted by soil texture, soil depth and amount of rainfall. This approach has the advantage of mapping RZSM at very high spatial resolution thanks to the SSM Sentinel-1 product. The current accuracy is encouraging considering the simplicity of the approach. However, the results of this study highlight significant potential for improvement, including: (i) The integration of soil, vegetation and climate variables into T calibration using machine learning algorithms; (ii) The use of enhanced quality SSM products derived from future L-band SAR missions; (iii) Mapping of wilting point and field capacity using a piecewise model.

CRedit authorship contribution statement

Ouaadi Nadia: Writing – review & editing, Writing – original draft, Visualization, Validation, Methodology, Investigation, Formal analysis, Data curation, Conceptualization. **Chehbouni Abdelghani:** Writing – review & editing, Funding acquisition, Conceptualization. **Ayari Emna:** Writing – review & editing, Formal analysis. **Boone Aaron:** Writing – review & editing, Formal analysis, Data curation. **Ait Hssaine Bouchra:** Writing – review & editing, Formal analysis. **ElFarkh Jamal:** Writing – review & editing, Formal analysis. **Le Page Michel:** Data curation. **Er-Raki Salah:** Data curation.

Declaration of Competing Interest

The authors declare that they have no known competing financial interests or personal relationships that could have appeared to influence the work reported in this paper.

Acknowledgement

This study was conducted within the framework of the Center of Remote Sensing Applications (CRSA) and funded by the OCP S.A. (Office Chérifien des Phosphates). The authors would like to thank the support of LMI TREMA (<http://trema.ucam.ac.ma/>), ANR-19-CE01-0017 HILIAISE project, EOAFRICA THESM project, the AfOEP CRSA-UM6P and MIT project (grant N°89) and FIRMA project (Grant n°AS140).

Appendix

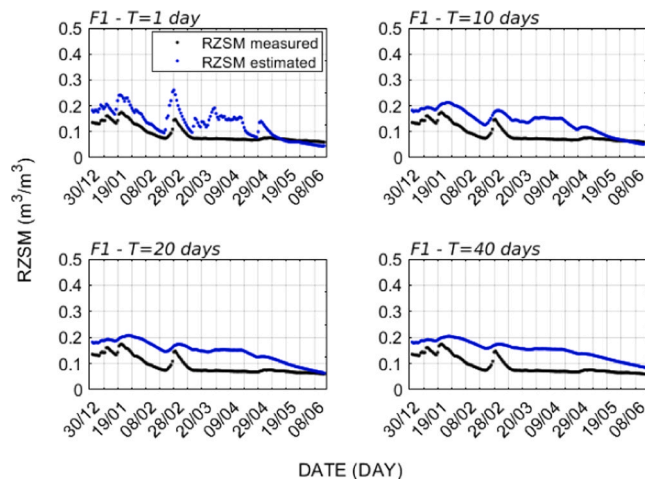


Fig. A1. Time series of F1 observed and estimated RZSM at 15 cm depth for four T values: 1 day, 10, 20 and 40 days

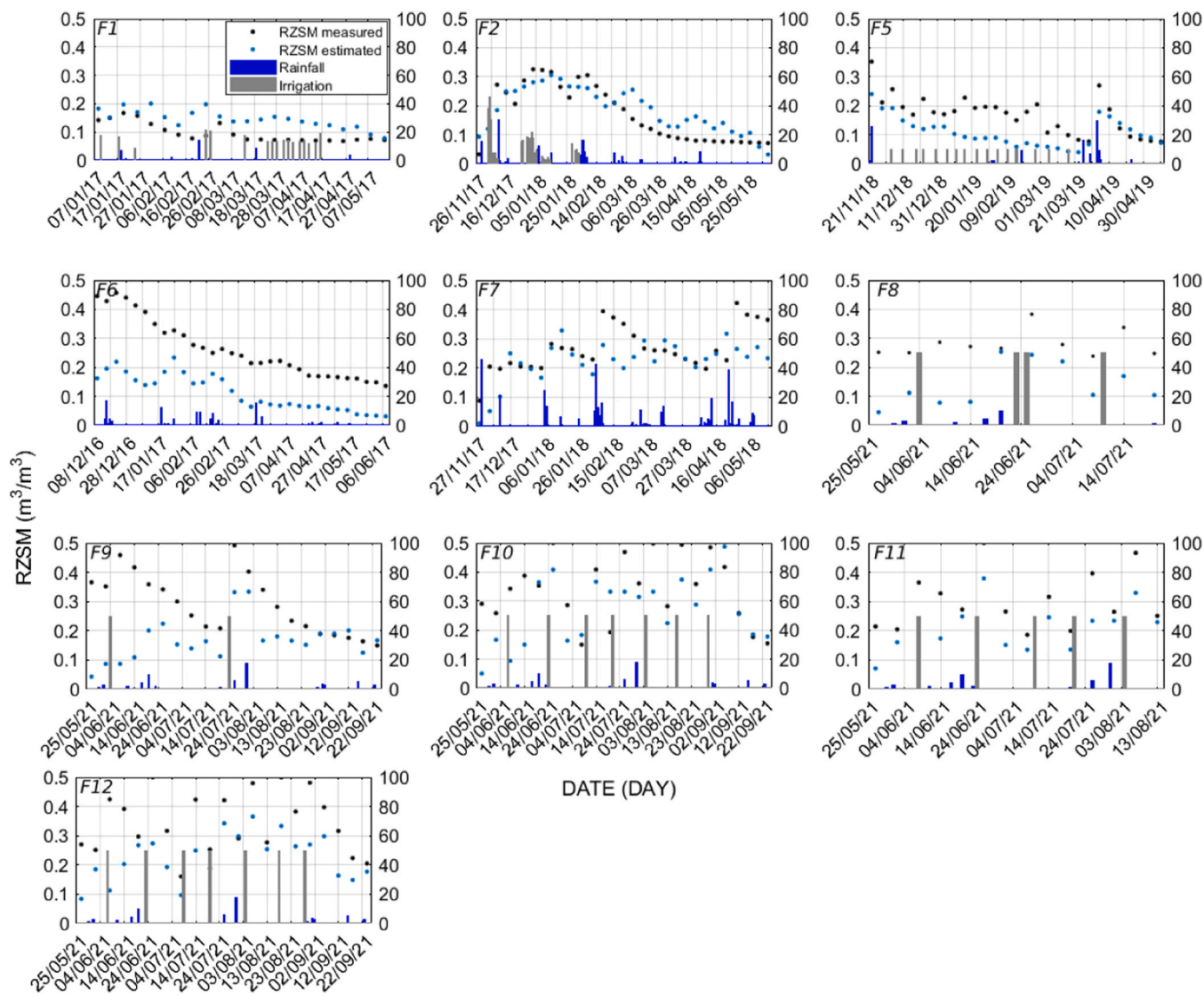


Fig. A2. Time series of the estimated and measured RZSM at 10–20 cm depth for all fields using Sentinel-1 SSM product

Data availability

Data will be made available on request.

References

- Ait Hssaine, B., Chehbouni, A., Er-raki, S., Khabba, S., Ezzahar, J., Ouadi, N., Ojha, N., Rivalland, V., Merlin, O., 2021. On the UTility Of High-resolution Soil Moisture Data For Better Constraining Thermal-based Energy Balance Over Three Semi-arid Agricultural Areas. *Remote Sens* 13, 727. <https://doi.org/10.3390/rs13040727>.
- Akbar, R., Short Gianotti, D.J., McColl, K.A., Haghighi, E., Salvucci, G.D., Entekhabi, D., 2018. Estimation of landscape soil water losses from satellite observations of soil moisture. *J. Hydrometeorol* 19, 871–889. <https://doi.org/10.1175/JHM-D-17-0200.1>.
- Albergel, C., Rüdiger, C., Pellarin, T., Calvet, J.C., Fritz, N., Froissard, F., Suquia, D., Petitpa, A., Pignat, B., Martin, E., 2008. From near-surface to root-zone soil moisture using an exponential filter: An assessment of the method based on in-situ observations and model simulations. *Hydrol. Earth Syst. Sci.* 12, 1323–1337. <https://doi.org/10.5194/hess-12-1323-2008>.
- Alfieri, L., Claps, P., D'Odorico, P., Laio, F., Over, T.M., 2008. An analysis of the soil moisture feedback on convective and stratiform precipitation. *J. Hydrometeorol.* 9, 280–291. <https://doi.org/10.1175/2007JHM863.1>.
- Ali, S., Xu, Y., Ma, X., Ahmad, I., Manzoor, Jia, Q., Akmal, M., Hussain, Z., Arif, M., Cai, T., Zhang, J., Jia, Z., 2019. Deficit irrigation strategies to improve winter wheat productivity and regulating root growth under different planting patterns. *Agric. Water Manag* 219, 1–11. <https://doi.org/10.1016/j.agwat.2019.03.038>.
- Attema, E.P.W., Ulaby, F.T., 1978. Vegetation modeled as a water cloud. *Radio Sci.* 13, 357–364. <https://doi.org/10.1029/RS013i002p00357>.
- Ayari, E., Kassouk, Z., Lili-chabaane, Z., Ouadi, N., Baghdadi, N., Zribi, M., 2024. NDVI estimation using Sentinel-1 data over wheat fields in a semiarid Mediterranean region. *GIScience Remote Sens* 61, 2357878. <https://doi.org/10.1080/15481603.2024.2357878>.
- Ayari, E., Zribi, M., Lili-Chabaane, Z., Kassouk, Z., Jarlan, L., Rodriguez-Fernandez, N., Baghdadi, N., 2023. Sensitivity of surface soil moisture retrieval to satellite-derived vegetation descriptors over wheat fields in the Kairouan plain. *Eur. J. Remote Sens* 56. <https://doi.org/10.1080/22797254.2023.2260555>.
- Babaeian, E., Paheding, S., Siddique, N., Devabhaktuni, V.K., Tuller, M., 2021. Estimation of root zone soil moisture from ground and remotely sensed soil information with multisensor data fusion and automated machine learning. *Remote Sens. Environ.* 260, 112434. <https://doi.org/10.1016/j.rse.2021.112434>.
- Bai, X., He, B., Li, X., Zeng, J., Wang, X., Wang, Z., Zeng, Y., Su, Z., 2017. First assessment of Sentinel-1A data for surface soil moisture estimations using a coupled water cloud model and advanced integral equation model over the Tibetan Plateau. *Remote Sens* 9, 1–20. <https://doi.org/10.3390/rs9070714>.
- Baldwin, D., Manfreda, S., Keller, K., Smithwick, E.A.H., 2017. Predicting root zone soil moisture with soil properties and satellite near-surface moisture data across the conterminous United States. *J. Hydrol.* 546, 393–404. <https://doi.org/10.1016/j.jhydrol.2017.01.020>.
- Blonquist, J.M., Jones, S.B., Robinson, D.A., 2006. Precise irrigation scheduling for turfgrass using a subsurface electromagnetic soil moisture sensor. *Agric. Water Manag* 84, 153–165. <https://doi.org/10.1016/j.agwat.2006.01.014>.
- Boone, A., Bellvert, J., Best, M., Brooke, J.K., Canut-Rocafort, G., Cuxart, J., Hartogensis, O., Le Moigne, P., Miró, J.R., Polcher, J., Price, J., Seguí, P.Q., Bech, J., Bezombes, Y., Branch, O., Cristóbal, J., Dassas, K., Fanise, P., Gibert, F., Goulas, Y., Groh, J., Hanus, J., Hmimina, G., Jarlan, L., Kim, E., Dantec, V., Le Page, L., Lohou, F., Lohou, M., Mangani, M.R., Martí, B., Martínez-Villagrasa, D., McGregor, J., Kerr-Munslow, A., Ouadi, N., Philibert, A., Quiros-Vargas, J., Rascher, U., Siegmann, B., Udina, M., Vial, A., Wrenger, B., Wulfmeyer, V., Zribi, M., 2025. The land surface interactions with the atmosphere over the iberian semi-arid environment (LIAISE) field campaign. *J. Eur. Meteorol. Soc. J. Eur. Meteorol. Soc.* 2, 100007. <https://doi.org/10.1016/j.jemets.2025.100007>.
- Brakhasi, F., Walker, J.P., Ye, N., Wu, X., Shen, X., Yeo, I.Y., Boopathi, N., Kim, E., Kerr, Y., Jackson, T., 2023. Towards soil moisture profile estimation in the root zone using L- and P-band radiometer observations: a coherent modelling approach. *Sci. Remote Sens* 7, 100079. <https://doi.org/10.1016/j.jrs.2023.100079>.
- Camillo, P., Schmugge, T.J., 1983. Estimating soil moisture storage in the root zone from surface measurements. *Soil Sci.* 135, 245–264. <https://doi.org/10.1097/00010694-198304000-00006>.
- Carlson, N.L., 1967. Dielectric constant of vegetation at 8.5 GHz. Columbus, Ohio.
- Carranza, C., Nolet, C., Peziz, M., van der Ploeg, M., 2021. Root zone soil moisture estimation with Random Forest. *J. Hydrol.* 593, 125840. <https://doi.org/10.1016/j.jhydrol.2020.125840>.
- Ceballos, A., Scipal, K., Wagner, W., Martínez-Fernández, J., 2005. Validation of ERS scatterometer-derived soil moisture data in the central part of the Duero Basin, Spain. *Hydrol. Process* 19, 1549–1566. <https://doi.org/10.1002/hyp.5585>.
- CEOS, 2024. Mission Summary - BIOMASS. URL (<https://database.eohandbook.com/database/missionsummary.aspx?MISSIONID=768>).
- Chen, Y., Lu, D., Luo, L., Pokhrel, Y., Deb, K., Huang, J., Ran, Y., 2018. Detecting irrigation extent, frequency, and timing in a heterogeneous arid agricultural region using MODIS time series, Landsat imagery, and ancillary data. *Remote Sens. Environ.* 204, 197–211. <https://doi.org/10.1016/j.rse.2017.10.030>.
- Das, K., Kumar, P., 2015. Present status of soil moisture estimation by microwave remote sensing. *Cogent Geosci.* 1, 1084669. <https://doi.org/10.1080/23312041.2015.1084669>.
- Das, N.N., Mohanty, B.P., 2006. Root zone soil moisture assessment using remote sensing and vadose zone modeling. *Vadose Zo. J.* 5, 296–307. <https://doi.org/10.2136/vzj2005.0033>.
- De Lange, R., Beck, R., Van De Giesen, N., Friesen, J., De Wit, A., Wagner, W., 2008. Scatterometer-derived soil moisture calibrated for soil texture with a one-dimensional water-flow model. *IEEE Trans. Geosci. Remote Sens* 46, 4041–4049. <https://doi.org/10.1109/TGRS.2008.2000796>.
- Dobrylaj, P., Qureshi, A., Badola, R., Hussain, S.A., 2012. A review of the methods available for estimating soil moisture and its implications for water resource management. *J. Hydrol.* 458–459, 110–117. <https://doi.org/10.1016/j.jhydrol.2012.06.021>.
- Dobson, M.C., Ulaby, F.T., 1986. Active microwave soil moisture research. *IEEE Trans. Geosci. Remote Sens.* GE 24, 23–36. <https://doi.org/10.1109/TGRS.1986.289585>.
- Dong, J., Akbar, R., Feldman, A.F., Gianotti, D.S., Entekhabi, D., 2023. Land surfaces at the tipping-point for water and energy balance coupling. *Water Resour. Res.* 59, e2022WR032472. <https://doi.org/10.1029/2022WR032472>.
- Dumedah, G., Walker, J.P., Merlin, O., 2015. Root-zone soil moisture estimation from assimilation of downscaled soil moisture and ocean salinity data. *Adv. Water Resour.* 84, 14–22. <https://doi.org/10.1016/j.advwatres.2015.07.021>.
- Ehdaie, B., Merhaut, D.J., Ahmadian, S., Hoops, A.C., Khuong, T., Layne, A.P., Waines, J. G., 2010. Root system size influences water-nutrient uptake and nitrate leaching potential in wheat. *J. Agron. Crop Sci.* 196, 455–466. <https://doi.org/10.1111/j.1439-037X.2010.00433.x>.
- El Hajj, M., Baghdadi, N., Zribi, M., Bazzi, H., 2017. Synergic use of Sentinel-1 and Sentinel-2 images for operational soil moisture mapping at high spatial resolution over agricultural areas. *Remote Sens* 9, 1–28. <https://doi.org/10.3390/rs9121292>.
- Entekhabi, B.D., Njoku, E.G., Neill, P.E.O., Kellogg, K.H., Crow, W.T., Edelstein, W.N., Entin, J.K., Goodman, S.D., Jackson, T.J., Johnson, J., Kimball, J., Piepmeier, J.R., Koster, R.D., Martin, N., McDonald, K.C., Moghaddam, M., Moran, S., Reichle, R., Shi, J.C., Spencer, M.W., Thurman, S.W., Tsang, L., Zyl, J.V., 2010. The SoilMoistureActivePassive (SMAP). : *IEEE Proc.* 704–716.
- ESA, 2024. ESA - Sentinel-1C captures first radar images. URL (https://www.esa.int/Applications/Observing_the_Earth/Copernicus/Sentinel-1/Sentinel-1C_captures_first_radar_images) (accessed 4.11.25).
- Etmiman, A., Tabatabaenejad, A., Moghaddam, M., 2020. Retrieving root-zone soil moisture profile from p-band radar via hybrid global and local optimization. *IEEE Trans. Geosci. Remote Sens* 58, 5400–5408. <https://doi.org/10.1109/TGRS.2020.2965569>.
- European Commission, Directorate-General for Defence Industry and Space, 2024. Waving goodbye to 2024 with another successful Copernicus Launch: Sentinel-1C now in orbit. URL (https://defence-industry-space.ec.europa.eu/waving-goodbye-2024-another-successful-copernicus-launch-sentinel-1c-now-orbit-2024-12-06_en) (accessed 4.11.25).
- Ezzahar, J., Chehbouni, A., Ouadi, N., Madiafi, M., Khabba, S., Er-Raki, S., Laamrani, A., Chakir, A., Chabaane, Z.L., Zribi, M., 2023. Sentinel-1 backscatter and interferometric coherence for soil moisture retrieval in winter wheat fields within a semi-arid south-mediterranean climate: machine learning versus semi-empirical models. *IEEE J. Sel. Top. Appl. Earth Obs Remote Sens.* 17, 2256–2271. <https://doi.org/10.1109/JSTARS.2023.3339616>.
- Fan, J., McConkey, B., Wang, H., Janzen, H., 2016. Root distribution by depth for temperate agricultural crops. *F. Crop. Res.* 189, 68–74. <https://doi.org/10.1016/j.fcr.2016.02.013>.
- Fang, Y., Liang, L., Liu, S., Xu, B., Siddique, K.H., Palta, J.A., Chen, Y., 2021. Wheat cultivars with small root length density in the topsoil increased post-anthesis water use and grain yield in the semi-arid region on the Loess Plateau. *Eur. J. Agron.* 124. <https://doi.org/10.1016/j.eja.2021.126243>.
- Ferguson, C.R., Pan, M., Oki, T., 2018. The effect of global warming on future water availability: CMIP5 synthesis. *Water Resour. Res.* 54, 7791–7819. <https://doi.org/10.1029/2018WR022792>.
- Fontanet, M., Fernández-García, D., Ferrer, F., 2018. The value of satellite remote sensing soil moisture data and the DISPATCH algorithm in irrigation fields. *Hydrol. Earth Syst. Sci.* 22, 5889–5900. <https://doi.org/10.5194/hess-22-5889-2018>.
- Ford, T.W., Harris, E., Quiring, S.M., 2014. Estimating root zone soil moisture using near-surface observations from SMOS. *Hydrol. Earth Syst. Sci.* 18, 139–154. <https://doi.org/10.5194/hess-18-139-2014>.
- González-Zamora, Á., Sánchez, N., Martínez-Fernández, J., Wagner, W., 2016. Root-zone plant available water estimation using the SMOS-derived soil water index. *Adv. Water Resour.* 96, 339–353. <https://doi.org/10.1016/j.advwatres.2016.08.001>.
- Guber, A.K., Gish, T.J., Pachepsky, Y.A., van Genuchten, M.T., Daughtry, C.S.T., Nicholson, T.J., Cady, R.E., 2008. Temporal stability in soil water content patterns across agricultural fields. *Catena* 73, 125–133. <https://doi.org/10.1016/j.catena.2007.09.010>.
- Hodgkinson, L., Dodd, I.C., Binley, A., Ashton, R.W., White, R.P., Watts, C.W., Whalley, W.R., 2017. Root growth in field-grown winter wheat: some effects of soil conditions, season and genotype. *Eur. J. Agron.* 91, 74–83. <https://doi.org/10.1016/j.eja.2017.09.014>.
- Huang, S., Ding, J., Zou, J., Liu, B., Zhang, J., Chen, W., 2019. Soil moisture retrieval based on sentinel-1 imagery under sparse vegetation coverage. *Sens. (Switz.)* 19, 1–18. <https://doi.org/10.3390/s19030589>.
- IPCC, 2019. Climate Change and Land: an IPCC special report on climate change, desertification, land degradation, sustainable land management, food security, and greenhouse gas fluxes in terrestrial ecosystems.
- Jarlan, L., Khabba, S., Szczypta, C., Lili-Chabaane, Z., Driouech, F., Le Page, M., Hanich, L., Fakir, Y., Boone, A., Boulet, G., 2016. Water resources in South Mediterranean catchments Assessing climatic drivers and impacts, in: *The Mediterranean Region under Climate Change*. IRD Edition, Marseille, pp. 303–309.

- Jiang, G., Wang, N., Zhang, Yaoyu, Wang, Z., Zhang, Yuling, Yu, J., Zhang, Yong, Wei, Z., Xu, Y., Geisen, S., Friman, V.P., Shen, Q., 2021. The relative importance of soil moisture in predicting bacterial wilt disease occurrence. *Soil Ecol. Lett.* 3, 356–366. <https://doi.org/10.1007/s42832-021-0086-2>.
- Kerr, Y.H., Waldteufel, P., Wigneron, J.-P., Martinuzzi, J., Font, J., Berger, M., 2001. Soil moisture retrieval from space: the soil moisture and ocean salinity (SMOS) mission. *IEEE Trans. Geosci. Remote Sens* 39, 1729–1735. <https://doi.org/10.1109/36.942551>.
- Khandan, R., Wigneron, J.P., Bonafoni, S., Biazar, A.P., Gholamnia, M., 2022. Assimilation of Satellite-Derived Soil Moisture and Brightness Temperature in Land Surface Models: A Review. *Remote Sens* 14, 1–32. <https://doi.org/10.3390/rs14030770>.
- Kim, Y., Park, H., Kimball, J.S., Colliander, A., McCabe, M.F., 2023. Global estimates of daily evapotranspiration using SMAP surface and root-zone soil moisture. *Remote Sens. Environ.* 298, 113803. <https://doi.org/10.1016/j.rse.2023.113803>.
- Koster, R.D., Dirmeyer, P.A., Guo, Z., Bonan, G., Chan, E., Cox, P., Gordon, C.T., Kanae, S., Kowalczyk, E., Lawrence, D., Liu, P., Lu, C.-H., Malyshev, S., McAvaney, B., Mitchell, K., Mocko, D., Oki, T., Oleson, K., Pitman, A., Sud, Y.C., Taylor, C.M., Verseghy, D., Vasic, R., Xue, Y., Yamada, T., 2004. Regions of strong coupling between soil moisture and precipitation, 1183–1141 *Science* 305 (80). <https://doi.org/10.1126/science.1100217>.
- Kostov, K.G., Jackson, T.J., 1993. layer is required. Conventional methods for soil moisture determination are time and labor tsuming and are remote sensing of soil moisture is the strong dependence of the soil ' s dielectric properties on its moisture conducted to understand the nature o 1941.
- Lal, P., Singh, G., Das, N.N., Entekhabi, D., Lohman, R., Colliander, A., Kumar, D., Setia, R.K., 2023. Remote sensing of environment a multi-scale algorithm for the NISAR mission high-resolution soil moisture product. *Remote Sens. Environ.* 295, 113667. <https://doi.org/10.1016/j.rse.2023.113667>.
- Laluet, P., Olivera-Guerra, L.E., Altés, V., Paolini, G., Ouaadi, N., Rivalland, V., Jarlan, L., Villar, J.M., Merlin, O., 2024. Retrieving the irrigation actually applied at district scale: assimilating high-resolution Sentinel-1-derived soil moisture data into a FAO-56-based model. *Agric. Water Manag* 293, 108704. <https://doi.org/10.1016/j.agwat.2024.108704>.
- Lannini, L., Davidson, M.W.J., Osborne, S., Gebert, N., Cosimo, G., Di, Mezzasoma, S., Petrolati, D., Kazimierczak, D., Arranz, C.D.L.F., Miccoli, A., Rojek, A., Nardecchia, L., Pavia, P., 2024. ROSE-L - the copernicus expansion L-band SAR mission. : *Eur. Conf. Synth. Aperture Radar*.
- Lesiv, M., Laso Bayas, J.C., See, L., Duerauer, M., Dahlia, D., Durando, N., Hazarika, R., Kumar Sahariah, P., Vakolyuh, M., Blyshchuk, V., Bilous, A., Perez-Hoyos, A., Gengler, S., Prestele, R., Bilous, S., Akhtar, I., ul, H., Singha, K., Choudhury, S.B., Chetri, T., Malek, Z., Bungnamei, K., Saikia, A., Sahariah, D., Narzary, W., Danylo, O., Sturm, T., Karner, M., McCallum, I., Schepaschenko, D., Moltchanova, E., Fraisl, D., Moorthy, I., Fritz, S., 2019. Estimating the global distribution of field size using crowdsourcing. *Glob. Chang. Biol.* 25, 174–186. <https://doi.org/10.1111/gcb.14492>.
- Li, Z.L., Leng, P., Zhou, C., Chen, K.S., Zhou, F.C., Shang, G.F., 2021. Soil moisture retrieval from remote sensing measurements: Current knowledge and directions for the future. *Earth-Sci. Rev.* 218, 103673. <https://doi.org/10.1016/j.earscirev.2021.103673>.
- Li, M., Sun, H., Zhao, R., 2023. A review of root zone soil moisture estimation methods based on remote sensing. *Remote Sens* 15, 1–23. <https://doi.org/10.3390/rs15225361>.
- Li, Y., Zhu, H., Li, J., Jin, H., Lu, B., Pan, X., 2021. Comparison of winter wheat (*Triticum aestivum* L.) root length density distribution models under salt stress. *Rhizosphere* 20, 100452. <https://doi.org/10.1016/j.rhisph.2021.100452>.
- Liu, E., Zhu, Y., Calvet, J.C., Lü, H., Bonan, B., Zheng, J., Gou, Q., Wang, X., Ding, Z., Xu, H., Pan, Y., Chen, T., 2024. Evaluation of root zone soil moisture products over the Huai River basin. *Hydrol. Earth Syst. Sci.* 28, 2375–2400. <https://doi.org/10.5194/hess-28-2375-2024>.
- Mahmood, R., Littell, A., Hubbard, K.G., You, J., 2012. Observed data-based assessment of relationships among soil moisture at various depths, precipitation, and temperature. *Appl. Geogr.* 34, 255–264. <https://doi.org/10.1016/j.apgeog.2011.11.009>.
- Maraseni, T.N., Pandey, S.S., 2014. Can vegetation types work as an indicator of soil organic carbon ? An insight from native vegetations in Nepal. *Ecol. Indic.* 46, 315–322. <https://doi.org/10.1016/j.ecolind.2014.06.038>.
- Martínez-Fernández, J., Ceballos, A., 2003. Temporal stability of soil moisture in a large-field experiment in Spain. *Soil Sci. Soc. Am. J.* 67, 1647–1656. <https://doi.org/10.2136/SSSAJ2003.1647>.
- Massari, C., Modanesi, S., Dari, J., Gruber, A., M., G.J., Lannoy, D., Giroto, M., Quintana-Seguí, P., Le Page, M., Jarlan, L., Zribi, M., Ouaadi, N., Vreugdenhil, M., Zappa, L., Dorigo, W., Wolfgang, W., Brombacher, J., Pelgrum, H., Jaquot, P., Freeman, V., Volden, E., Prieto, D.F., Tarpanelli, A., Barbetta, S., Brocca, L., 2021. A review of irrigation information retrievals from space and their utility for users. *Remote Sens* 13. <https://doi.org/10.3390/rs13204112>.
- Mawodza, T., Burca, G., Casson, S., Menon, M., 2020. Wheat root system architecture and soil moisture distribution in an aggregated soil using neutron computed tomography. *Geoderma* 359. <https://doi.org/10.1016/j.geoderma.2019.113988>.
- McDermid, S., Nocco, M., Lawston-Parker, P., Keune, J., Pokhrel, Y., Jain, M., Jägermeyr, J., Brocca, L., Massari, C., Jones, A.D., Vahmani, P., Thiery, W., Yao, Y., Bell, A., Chen, L., Dorigo, W., Hanasaki, N., Jasechko, S., Lo, M.-H., Mahmood, R., Mishra, V., Mueller, N.D., Niyogi, D., Rabin, S.S., Sloat, L., Wada, Y., Zappa, L., Chen, F., Cook, B.L., Kim, H., Lombardozi, D., Polcher, J., Ryu, D., Santanello, J., Satoh, Y., Seneviratne, S., Singh, D., Yokohata, T., 2023. Irrigation in the earth system. *Nat. Rev. Earth Environ.* <https://doi.org/10.1038/s43017-023-00438-5>.
- MedECC, 2020. Climate and Environmental Change in the Mediterranean basin.
- Montavon, G., Samek, W., Müller, K.R., 2018. Methods for interpreting and understanding deep neural networks. *Digit. Signal Process. A Rev. J.* 73, 1–15. <https://doi.org/10.1016/j.dsp.2017.10.011>.
- Moran, M.S., Peters-Lidard, C.D., Watts, J.M., Mc Elroy, S., 2004. Estimating soil moisture at the watershed scale with satellite-based radar and land surface models. *Can. J. Remote Sens* 30, 805–826. <https://doi.org/10.5589/m04-043>.
- Namdari, H., Moradikia, M., Zekavat, S., Askari, R., Mangoubi, O., Petkie, D., 2024. Advancing precision agriculture: machine learning-enhanced GPR analysis for root-zone soil moisture assessment in mega farms. *IEEE Trans. Agric. Electron* 1–12. <https://doi.org/10.1109/TAFE.2024.3455238>.
- NISAR, 2019. NISAR: The NASA-ISRO SAR Mission. Pasadena, California.
- Njoku, E.G., Jackson, T.J., Lakshmi, V., Chan, T.K., Nghiem, S.V., 2003. Soil moisture retrieval from AMSR-E. *IEEE Trans. Geosci. Remote Sens* 41, 215–228. <https://doi.org/10.1109/TGRS.2002.808243>.
- Noborio, K., 2001. Measurement of soil water content and electrical conductivity by time domain reflectometry: a review. *Comput. Electron. Agric.* 31, 213–237. [https://doi.org/10.1016/S0168-1699\(00\)00184-8](https://doi.org/10.1016/S0168-1699(00)00184-8).
- Oh, Y., Sarabandi, K., Ulaby, F.T., 1992. An empirical model and an inversion technique for radar scattering from bare soil surfaces. *IEEE Trans. Geosci. Remote Sens* 30, 370–381. <https://doi.org/10.1109/36.134086>.
- Ouaadi, N., Ezzahar, J., Khabba, S., Er-Raki, S., Chakir, A., Ait Hssaine, B., Le Dantec, V., Rafi, Z., Beaumont, A., Kasbani, M., Jarlan, L., 2021a. C-band radar data and in situ measurements for the monitoring of wheat crops in a semi-arid area (center of Morocco). *Earth Syst. Sci. Data* 13, 3707–3731. <https://doi.org/10.5194/essd-13-3707-2021>.
- Ouaadi, N., Jarlan, L., Ezzahar, J., Zribi, M., Khabba, S., Bouras, E., Bousbih, S., Frison, P., 2020. Monitoring of wheat crops using the backscattering coefficient and the interferometric coherence derived from Sentinel-1 in semi-arid areas. *Remote Sens. Environ.* 251, 112050. <https://doi.org/10.1016/j.rse.2020.112050>.
- Ouaadi, N., Jarlan, L., Khabba, S., Ezzahar, J., Le Page, M., Merlin, O., 2021b. Irrigation amounts and timing retrieval through data assimilation of surface soil moisture into the FAO-56 approach in the South Mediterranean Region. *Remote Sens* 13, 2667.
- Ouaadi, N., Jarlan, L., Khabba, S., Le Page, M., Chakir, A., Er-raki, S., Frison, P.L., 2023. Are the C-band backscattering coefficient and interferometric coherence suitable substitutes of NDVI for the monitoring of the FAO-56 crop coefficient. *Agric. Water Manag* 282, 108276. <https://doi.org/10.1016/j.agwat.2023.108276>.
- Ouaadi, N., Jarlan, L., Le Page, M., Zribi, M., Paolini, G., Ait Hssaine, B., Escorihuela, M. J., Fanise, P., Merlin, O., Baghdadi, N., Boone, A., 2024a. Intercomparison of very high-resolution surface soil moisture products over Catalonia (Spain). *Remote Sens. Environ.* 309, 114225. <https://doi.org/10.1016/j.rse.2024.114225>.
- Ouaadi, N., Jarlan, L., Villard, L., Chakir, A., Khabba, S., Fanise, P., Kasbani, M., Rafi, Z., Le, V., Ezzahar, J., Frison, L., 2024b. Temporal decorrelation of C-band radar data over wheat in a semi-arid area using sub-daily tower-based observations. *Remote Sens. Environ.* 304, 114059. <https://doi.org/10.1016/j.rse.2024.114059>.
- Pablos, M., González-Zamora, A., Sánchez, N., Martínez-Fernández, J., 2018. Assessment of root zone soil moisture estimations from SMAP, SMOS and MODIS observations. *Remote Sens* 10. <https://doi.org/10.3390/rs10070981>.
- Paloscia, S., Pettinato, S., Santi, E., Notarnicola, C., Pasolli, L., Reppucci, A., 2013. Soil moisture mapping using Sentinel-1 images: algorithm and preliminary validation. *Remote Sens. Environ.* 134, 234–248. <https://doi.org/10.1016/j.rse.2013.02.027>.
- Paolini, G., Escorihuela, M.J., Bellvert, J., Merlin, O., 2022. Disaggregation of SMAP soil moisture at 20 m resolution: validation and sub-field scale analysis. *Remote Sens* 14, 1–16. <https://doi.org/10.3390/rs14010167>.
- Pasik, A., Gruber, A., Preimesberger, W., De Santis, D., Dorigo, W., 2023. Uncertainty estimation for a new exponential-filter-based long-Term root-zone soil moisture dataset from Copernicus Climate Change Service (C3S) surface observations. *Geosci. Model Dev.* 16, 4957–4976. <https://doi.org/10.5194/gmd-16-4957-2023>.
- Paulik, C., Dorigo, W., Wagner, W., Kidd, R., 2014. Validation of the ASCAT soil water index using in situ data from the International Soil moisture network. *Int. J. Appl. Earth Obs. Geoinf.* 30, 1–8. <https://doi.org/10.1016/j.jag.2014.01.007>.
- Picard, G., Toan, T.L., Mattia, F., 2003. Understanding C-band radar backscatter from wheat canopy using a multiple-scattering coherent model. *IEEE Trans. Geosci. Remote Sens* 41, 1583–1591. <https://doi.org/10.1109/TGRS.2003.813353>.
- Prasad, R., Deo, R.C., Li, Y., Maraseni, T., 2018. Soil moisture forecasting by a hybrid machine learning technique: ELM integrated with ensemble empirical mode decomposition. *Geoderma* 330, 136–161. <https://doi.org/10.1016/j.geoderma.2018.05.035>.
- Quegan, S., Le Toan, T., Chave, J., Dall, J., Exbrayat, J.F., Minh, D.H.T., Lomas, M., D'Alessandro, M.M., Paillou, P., Papathanassiou, K., Rocca, F., Saatchi, S., Scipal, K., Shugar, H., Smallman, T.L., Soja, M.J., Tebaldini, S., Ulander, L., Villard, L., Williams, M., 2019. The European Space Agency BIOMASS mission: measuring forest above-ground biomass from space. *Remote Sens. Environ.* 227, 44–60. <https://doi.org/10.1016/j.rse.2019.03.032>.
- Reichstein, M., Camps-Valls, G., Stevens, B., Jung, M., Denzler, J., Carvalhais, N., Prabhat, 2019. Deep learning and process understanding for data-driven Earth system science. *Nature* 566, 195–204. <https://doi.org/10.1038/s41586-019-0912-1>.
- Riedel, T., Pathe, C., Thiel, C., Herold, M., Schmulius, C., 2002. Systematic investigation on the effect of dew and interception on multifrequency and multipolarimetric radar backscatter signals, in: 3rd International Symposium, ' Retrieval of Bio- and Geo-Physical Parameters from SAR Data for Land Applications'. pp. 99–104.
- Sabater, J.M., Jarlan, L., Calvet, J.-C., Bouysse, F., 2007. From near-surface to root-zone soil moisture using different. *J. Hydrol.* 8, 194–206. <https://doi.org/10.1175/JHM571.1>.
- Souissi, R., Zribi, M., Corbari, C., Mancini, M., Muddu, S., Tomer, S.K., Upadhyaya, D.B., Al Bitar, A., 2022. Integrating process-related information into an artificial neural

- network for root-zone soil moisture prediction. *Hydrol. Earth Syst. Sci.* 26, 3263–3297. <https://doi.org/10.5194/hess-26-3263-2022>.
- Taylor, C.M., Parker, D.J., Harris, P.P., 2007. An observational case study of mesoscale atmospheric circulations induced by soil moisture. *Geophys. Res. Lett.* 34, 2–7. <https://doi.org/10.1029/2007GL030572>.
- Tian, J., Zhang, Y., Guo, J., Zhang, X., Ma, N., Wei, H., Tang, Z., 2022. Predicting root zone soil moisture using observations at 2121 sites across China. *Sci. Total Environ.* 847, 157425. <https://doi.org/10.1016/j.scitotenv.2022.157425>.
- Tobin, J.K., Torres, R., Crow, T.W., Bennett, E.M., 2017. Multi-decadal analysis of root-zone soil moisture applying the exponential filter across CONUS. *Hydrol. Earth Syst. Sci.* 21, 4403–4417. <https://doi.org/10.5194/hess-21-4403-2017>.
- Ulaby, F.T., Allen, C.T., Eger III, G., 1984. Relating the microwave backscattering coefficient to leaf area index. *Remote Sens. Environ.* 14, 113–133. [https://doi.org/10.1016/0034-4257\(84\)90010-5](https://doi.org/10.1016/0034-4257(84)90010-5).
- Ulaby, F.T., Dubois, P.C., Jakob, V.Z., 1996. Radar mapping of surface soil moisture. *J. Hydrol.* 184, 57–84.
- Ulaby, F.T., Moore, R.K., Fung, A.K., 1986. Microwave remote sensing: Active and Passive, Volume III—from theory to applications.
- United Nations, 2024. The United Nations World Water Development Report 2024: Water for Prosperity and Peace, The Paraná River Basin. Paris. <https://doi.org/10.4324/9780429317729-8>.
- Valayamkunnath, P., Sridhar, V., Zhao, W., Allen, R.G., 2019. A comprehensive analysis of interseasonal and interannual energy and water balance dynamics in semiarid shrubland and forest ecosystems. *Sci. Total Environ.* 651, 381–398. <https://doi.org/10.1016/j.scitotenv.2018.09.130>.
- Van Oorschot, F., Van Der Ent, R.J., Hrachowitz, M., Alessandri, A., 2021. Climate-controlled root zone parameters show potential to improve water flux simulations by land surface models. *Earth Syst. Dyn.* 12, 725–743. <https://doi.org/10.5194/esd-12-725-2021>.
- Vereecken, H., Huisman, J.A., Bogena, H., Vanderborght, J., Vrugt, J.A., Hopmans, J.W., 2008. On the value of soil moisture measurements in vadose zone hydrology: a review. *Water Resour. Res.* 46, 1–21. <https://doi.org/10.1029/2008WR006829>.
- Vereecken, H., Maes, J., Feyen, J., Darius, P., 1989. Estimating the soil moisture retention characteristic from texture, bulk density, and carbon content. *Soil Sci.* 148, 389–403. <https://doi.org/10.1097/00010694-198912000-00001>.
- Wagner, W., Lemoine, G., Rott, H., 1999. A method for estimating soil moisture from ERS Scatterometer and soil data. *Remote Sens. Environ.* 70, 191–207. [https://doi.org/10.1016/S0034-4257\(99\)00036-X](https://doi.org/10.1016/S0034-4257(99)00036-X).
- Wagner, W., Lindorfer, R., Melzer, T., Hahn, S., Bauer-Marschallinger, B., Morrison, K., Calvet, J.C., Hobbs, S., Quast, R., Greimeister-Pfeil, I., Vreugdenhil, M., 2022. Widespread occurrence of anomalous C-band backscatter signals in arid environments caused by subsurface scattering. *Remote Sens. Environ.* 276, 113025. <https://doi.org/10.1016/j.rse.2022.113025>.
- Wagner, W., Scipal, Klaus, Pathe, Carsten, Gerten, Dieter, Lucht, Wolfgang, Rudolf, Bruno, Wagner, C., Scipal, K., Pathe, C., Gerten, D., Lucht, W., Rudolf, B., 2003. Evaluation of the agreement between the first global remotely sensed soil moisture data with model and precipitation data. *J. Geophys. Res.* 108, 4611. <https://doi.org/10.1029/2003JD003663>.
- Wang, T., Franz, T.E., You, J., Shulski, M.D., Ray, C., 2017. Evaluating controls of soil properties and climatic conditions on the use of an exponential filter for converting near surface to root zone soil moisture contents. *J. Hydrol.* 548, 683–696. <https://doi.org/10.1016/j.jhydrol.2017.03.055>.
- Xu, H., Vandecasteele, B., Maenhout, P., Pannecoucq, J., De Neve, S., Sleutel, S., 2020. Maize root biomass and architecture depend on site but not on variety: consequences for prediction of C inputs and spread in topsoil based on root-to-shoot ratios. *Eur. J. Agron.* 119, 126121. <https://doi.org/10.1016/j.eja.2020.126121>.
- Ya'nan, Z., Binyao, W., Weiwei, Z.H.U., Li, F., Qisheng, H.E., Xin, Z., 2024. Spatial-temporal constraints for surface soil moisture mapping using Sentinel-1 and Sentinel-2 data over agricultural regions. *Comput. Electron. Agric.* 219, 108835. <https://doi.org/10.1016/j.compag.2024.108835>.
- Yang, Y., Bao, Z., Wu, H., Wang, G., Liu, C., Wang, J., Zhang, J., 2022. An exponential filter model-based root-zone soil moisture estimation methodology from multiple datasets. *Remote Sens.* 14, 1–22. <https://doi.org/10.3390/rs14081785>.
- Zeng, L., Hu, S., Xiang, D., Zhang, X., Li, D., Li, L., Zhang, T., 2019. Multilayer soil moisture mapping at a regional scale from multisource data via a machine learning method. *Remote Sens.* 11, 284. <https://doi.org/10.3390/rs11030284>.
- Zhao, D., Kuenzer, C., Fu, C., Wagner, W., 2008. Evaluation of the ERS scatterometer-derived soil water index to monitor water availability and precipitation distribution at three different scales in China. *J. Hydrometeorol.* 9, 549–562. <https://doi.org/10.1175/2007JHM965.1>.
- Zreda, M., Shuttleworth, W.J., Zeng, X., Zweck, C., Desilets, D., Franz, T., Rosolem, R., 2012. COSMOS: The cosmic-ray soil moisture observing system. *Hydrol. Earth Syst. Sci.* 16, 4079–4099. <https://doi.org/10.5194/hess-16-4079-2012>.